Lithospheric magma dynamics beneath the El Hierro Volcano, Canary Islands: insights from fluid inclusions

Lithospheric magma dynamics beneath El Hierro volcano, Canary Islands: insight from fluid inclusions

E. Oglialoro[1], M.L. Frezzotti[1], S. Ferrando[2], C. Tiraboschi[1], C. Principe[3], G. Groppelli[4], I.M. Villa,[1,5,6]

1-Dipartimento di Scienze dell'Ambiente e della Terra, Università di Milano Bicocca, 20126 Milan, Italy
2-Dipartimento di Scienze della Terra, Università di Torino, 70125 Turin, Italy
3-Istituto di Geoscienze e Georisorse, Consiglio Nazionale delle Ricerche, 56121 Pisa, Italy
4-Istituto per la Dinamica dei Processi Ambientali-sezione di Milano, Consiglio Nazionale delle Ricerche, 20131 Milan, Italy
5-Institut für Geologie, Universität Bern, 3012 Bern, Switzerland
6-Centro Universitario Datazioni e Archeometria, Università di Milano Bicocca, 20126 Milano, Italy

Corresponding author: Maria Luce Frezzotti maria.frezzotti@unimib.it

Keywords El Hierro, petrology, fluid inclusions, mantle xenoliths, magma transport

Abstract

In active volcanoes, petrological studies have been proven to represent a reliable approach to defining the depth conditions of magma transport and storage in the mantle and the crust. Based on fluid inclusion mineral geothermobarometry in mantle xenoliths, we propose a model for the recent magma plumbing system of the Island of El Hierro (Canary Islands). Studied peridotites are entrained in a lava flow from El Yulan Valley, which is part of the Rift volcanism activity at approximately 40-30 ka. Peridotites are spinel lherzolites, harzburgites and dunites equilibrated in the shallow mantle at pressures from 1.5 to 2 GPa. 800 to 950°C (LT peridotites).

and higher equilibration temperatures from 900 to 1100°C (HT peridotites). Microthermometry and Raman analyses of fluid inclusions show trapping of two distinct fluid phases: early Type I metasomatic CO_2-N_2 fluids (d = 1.19 g/cm^3), coexisting with silicate-carbonate melts, in LT peridotites; and late Type II pure CO_2 fluids (d = 0.99 to 1.11 and 0.65 - 0.75 g/cm^3) in both LT and HT peridotites. Type I fluids represent metasomatic phases in the deep oceanic lithosphere (60-65 km) before the onset of magmatic activity, whereas Type II CO_2 fluids testify for fluid trapping episodes during the ascent of xenoliths in host mafic magmas. Identification of magma accumulation zones through interpretation of Type II CO_2 fluid inclusions and mineral geothermobarometry indicate the presence of a vertically stacked system of interconnected small magma reservoirs in the shallow lithospheric mantle from 22 to 36 km depth (or 0.67 to 1 GPa). This deeper magma accumulation region fed a short-lived magma storage region located in the lower oceanic crust at 10 - 12 km depth (or 0.26–0.34 GPa). According to our model, the 40-30 ka old volcanic activity of El Hierro is related to mantle magma dynamics, as also proposed for the 2011-2012 eruption.

Introduction

A central question for forecasting eruptive behavior in active volcanoes is the architecture of the magma plumbing system, which exerts a critical control on the compositional variation of magmas, the depths and conditions at which they are stored, and their residence time at different crustal/mantle levels (e.g., Sparks 2003; Peccerillo et al. 2006; Scandone et al. 2007).

Multiple and complementary studies combining both geophysical and petrological approaches are applied to get insights into the internal structure of volcanoes (e.g. Bertagnini et al. 2003; Schwarz et al. 2004; Morgan et al. 2007; Stroncik et al. 2009). Among petrological studies, fluid inclusion and mineral geothermobarometry provide information on the depths of magma ponding and crystallization (c.f. Andersen and Neumann 2001: Frezzotti and Peccerillo 2004; Hansteen and Klügel 2008). Fluid inclusions, in fact, record pressures of trapping at and changes of fluid density in response to magma pressure variations on short time scales (Peccerillo et al. 2006). They are therefore sensitive probes of discrete magma storage regions.

This approach has been successfully applied to several active volcanoes both in the oceanic and continental lithosphere (e.g., Hawaii, Canary Islands, Azores, and the Aeolian Islands; Roedder 1983; De Vivo et al. 1988, Frezzotti et al. 1991; Hansteen et al. 1998; Zanon et al. 2003; Zanon and Frezzotti 2013). In the Canary Islands, previous fluid inclusion studies suggested that the volcanoes are supplied by a plumbing system that delivers magma directly in the lower crust (e.g., Hansteen et al. 1991, 1998; Frezzotti et al. 1994; Andersen et al. 1995; Neumann et al. 1995; Viti and Frezzotti 2000; Klügel et al. 2005, 2015). Although fluid inclusion investigations have failed to identify magma storage regions below the Moho,

mineral-melt geothermobarometry indicates variable clinopyroxene crystallization from 15 to 45 km depth beneath La Palma and El Hierro (Stroncik et al. 2009; Barker et al. 2015; Klügel et al. 2015).

At El Hierro, multidisciplinary research, undertaken since the last submarine eruption of 2011-2012, has allowed identifying the presence of two discrete magma storage regions, located in the lower oceanic crust and the lithospheric mantle, respectively (Meletlidis et al. 2012; Becerill et al. 2013b; González et al. 2013; Martí et al. 2013a, b; Longpré et al. 2014; Klügel et al. 2015; Carracedo et al. 2015; Zaczek et al. 2015). As summarized by Klügel et al. (2015), eruptive magma transport in the oceanic crust is characterized by sub-horizontal and lateral pathways forming temporary deep sheet intrusions (sills). These are fed by a deeper reservoir in the shallow lithospheric mantle. However, the state of this sub-Moho magma storage region is not fully resolved (e.g., Martì et al. 2013a).

In this work, we concentrate on the reconstruction of the magma plumbing system of El Hierro volcano, focusing on magma storage in the oceanic lithospheric mantle. Following the approach of Frezzotti and Peccerillo (2004), we have performed geothermobarometry of fluid inclusions and minerals in ultramafic xenoliths from a lava flow of El Julan cliff, representative of the Rift Volcanism activity at approximately 40-30 ka (Guillou et al. 1996; Carracedo et al. 2001; Becerill et al. 2013a). Results allow modeling the internal structure of El Hierro volcano.

Geological setting

The Canary archipelago (Spain) consists of seven main volcanic islands located on the continental rise off Cape Juby (northwest Africa). It extends for roughly 500 km in a ridge

developed on the margin of the African Plate (Fig. 1a) (Robertson and Stillman 1979; Marinoni and Pasquarè 1994; Carracedo et al. 1999; Marinoni and Gudmundsson 2000).

The sub-aerial volcanic activity shows a general westwards decrease in age from 21-20 Ma at Fuerteventura-Lanzarote to less than 2 Ma at El Hierro and La Palma (Fig.1a), that are at present in their shield building phase (Schmincke 1982; Guillou et al. 1996; Carracedo 1999;). The islands lay on oceanic lithosphere formed during the opening of the Central Atlantic Ocean (~150-180 Ma; Hoernle 1998). The oceanic crust shows an eastward progressive thickening, from about 12 - 15 km at El Hierro to 35 km at Lanzarote (Martinez-Arevalo et al. 2013). The main regional tectonic structures have been classified in Atlantic or "oceanic" (N160–N180°E, N120–N135°E), and African or "continental" (N20°E, N45°E, N75°E) (Anguita and Hernan 1975, 2000; Füster 1975; Geyer and Martí 2010).

Magmatic activity is dominated by alkali-basalts (picrites, basanites), with minor tholeiites and differentiated lavas (e.g. trachytes and phonolites). The origin of intraplate volcanic activity is still controversial (cf. Lustrino and Wilson 2007). The most popular genetic hypothesis is the mantle plume model (e.g. Hoernle and Schminke 1993; Carracedo et al. 1998; Duggen et al. 2009), although other interpretations have been proposed, including a local extensional model (Füster 1975) and an uplifted tectonic block model (Araña and Ortiz 1991). Moreover, Anguita and Hernán (2000) postulated a single unified model taking into account mantle plume dynamics combined with the regional tectonics to explain the initiation of mantle melting processes.

At El Hierro, the sub-aerial volcanic activity started at 1.12 Ma, with massive lava flows in the NE of the island (Guillou et al. 1996). Three main volcanic cycles are identified, namely Tiñor Edifice (1.12-0.88 Ma), Golfo-Las Playas Edifice (0.545-0.176 Ma), and Rift Volcanism (0.158 Ma - Present) (Carracedo et al. 2001; IGME 2010a, b, c, d; Becerril et al.

2013a). These cycles are separated by quiescence, structural deformation and sector collapses. Sector collapses formed four main amphitheaters: Las Playas I and II (~545-0.176 and 0.176-0.145 Ma, respectively), El Julan (~ 0.158 Ma) and the Golfo (~ 87-39 ka) (Masson 1996; Masson et al. 2002; 2006; Gee et al. 2001; Longpré et al. 2011). Erupted lavas increase in alkalinity and degree of evolution through time (Stroncik et al. 2009). Lavas of Tiñor volcano are picritic to hawaiitic-tephritic in composition, whereas those of the Golfo-Las Playas edifice range from basanites to trachytes and nephelinites.

The last cycle of Rift Volcanism (158 ka - Present) is characterized by cinder cones and relatively thin lava flows covering most of the island. Lavas are mainly alkali-picrites and basanites with minor tephrites (Carracedo et al. 2001). Radiometric ages ranging from 158 to 2.5 ka broadly constrain the Rift Volcanism activity (Guillou et al. 1996; Carracedo et al. 2001). Over the last 600 years, a single submarine monogenic eruption occurred in La Restinga area in 2011-2012 (e.g. Lopez et al. 2012; Martí et al. 2013a, b; Longpré et al. 2014).

Abundant ultramafic xenoliths are reported in several lava flows and pyroclastic rocks on the Island (Neumann 1990, Hansteen et al. 1991; Neumann et al. 2004). For the present study, xenolith samples have been collected in a locality in the El Julan Cliff Valley (27°41'27"N - 18°02'49"W), not sampled before (Fig. 1b). The outcrop consists of a massive basaltic lava flow of about 3 m thickness (Fig. 2a), which is part of a continuous succession without any significant unconformity. No dating is available for this xenolith-bearing lava flow, but its position is compatible with the Rift Volcanism activity at approximately 40-30 ka. In fact, Carracedo et al. (2001) dated two lava flows in this area (~ 1 km southwest) at 41 and 31 ka, respectively (K-Ar dating).

142 **Analytical techniques**

143

144 Peridotite modal compositions have been defined by multicolor image analysis
145 (ImageJ and Photoshop C5 softwares), reconstructing the total pixel areas of minerals
146 identified in thin sections.

147 A Wavelength Dispersive System (WDS) microprobe has been used for major element
148 composition of mineral phases, using double-polished thick sections. WDS analyses have been
149 performed with a JEOL JXA 8200 Superprobe, equipped with five wavelength-dispersive
150 spectrometers, Energy Dispersive X-ray spectroscopy (EDS), and cathodoluminescence
151 detectors at the University of Milano. The operating conditions consist of an acceleration
152 voltage of 15 kV, at a beam current of 15 nA at 30s counting time, with a spot size of 1 μm.
153 The typical detection limit for each element was 0.01%. Natural and synthetic minerals have
154 been used as standards, within 2% at 2σ standard deviation. Structural formulae of minerals
155 have been processed through the software NORM of Ulmer (1986).

156 Fluid inclusion microthermometry has been carried out with a Linkam THMS600
157 heating/freezing stage, equipped with a Leitz microscope (40× objective), which operates in a
158 temperature range between -196 and 600°C at the University of Milano Bicocca. The
159 instrument was calibrated checking CO_2 and H_2O triple points (-56.6°C and 0.1°C,
160 respectively) in natural and synthetic fluid inclusions (SYN-FLINC). In the temperature
161 interval from -90 to 31°C, an accuracy of ± 0.1 °C has been estimated at the standard reference
162 points, and of ± 0.2 °C at the other temperatures. The melting temperature (Tm) and the
163 homogenization temperature (Th) of fluid inclusions have been measured with a heating rate
164 variable from 0.3 to 0.1 °C/min. The density of CO_2 inclusions has been calculated by the
165 equation of Duschek et al. (1990) (BULK software; Bakker 2003). Isochores have been

166 determined using the equation of Holloway (1981) (ISOCHORE software; Bakker 2003). The
167 selected equation is valid up to least 2000 °K and 1.5 GPa. Molar volumes of CO_2-N_2 fluids
168 have been derived by plotting fluid composition determined by Raman spectroscopy and
169 temperature of measured sequences of phase transitions in the isochoric (cm^3/mole) CO_2-N_2 T-
170 X diagram of van den Kerkhof (1988) and Klemd et al. (1992). Isochores for CO_2-N_2 fluid
171 inclusions have been calculated using the equation of Holloway (1977) valid from 373 to 1273
172 °K and up to 2 GPa, (ISOCHORE software; Bakker 2003).

173 Fluid inclusions have been further analyzed by Raman microspectroscopy (Horiba
174 Labram HR800) at the "G. Scansetti" Center of the University of Torino. A polarized Nd
175 green laser operating at 532 nm wavelength and 80 mW emission power was used as the
176 excitation source, with a spot size resolution of 1x1x3 μm. The slit width was 300 μm, the
177 grating was 600 grooves/mm, and the corresponding spectral resolution was ± 1.5 cm^{-1}.
178 Raman spectra have been collected with a 100× Olympus objective and 3 accumulations of
179 30s. The calibration of the instrument has been daily checked by the 521 cm^{-1} silicon band.
180 The determination of the relative molar fractions of end-member components in CO_2–N_2
181 mixtures, as well as the characterization of daughter minerals in fluid inclusions, have been
182 made following Frezzotti et al. (2012; and references therein). Spectra statistical fitting has
183 been performed with Fityk 0.9.8 free analysis software, applying PseudoVoigt functions.

184 The "Raman densimeter" (e.g. Rosso and Bodnar 1995) for pure CO_2 fluid inclusions,
185 based on the distance of the CO_2 Fermi doublet (Δ, in cm^{-1}; Wang and Wright 1973; Garrabos
186 et al. 1980) has been applied using the equation of Kawakami et al. (2003) with an accuracy
187 better than 5% in the density range from 0.1 to 1.24 g/cm^3. Selection of the Raman densimeter
188 equation was performed comparing CO_2 density values derived from microthermometry with
189 those calculated by Raman analyses applying existing equations (cf., Frezzotti et al. 2012) in

20 fluid inclusions. The equation of Kawakami et al. (2003) resulted as the most accurate for studied fluid inclusions.

Composition and P-T equilibration conditions of peridotites

Ultramafic xenoliths are angular in shape and about 8-10 cm in size on average (Fig. 2a). They have a pale green color, characteristic for fresh peridotites. The rock contours are sharp and lava infiltrations are generally absent. The host basanitic lava is unaltered, porphyritic, and consists of olivine and Ti-augite phenocrysts (30 vol%) in a glassy groundmass. Among collected samples, 11 peridotites have been selected for petrological and fluid inclusion studies.

Petrography and mineral chemistry of peridotites

Studied rocks are type I peridotites (Frey and Prinz 1978) and consist of 3 spinel dunites (Ol 92-94, Cpx 1-4, Opx 4-6 vol%; samples XML 1, 5, and 10), 3 spinel lherzolites (Ol 63-78, Cpx 11-12, Opx 11-26 vol%; samples XML 3, 6, and 8) and 5 spinel harzburgites (Ol 59-78, Cpx 2-4, Opx 18-38 vol%; samples XML 4, 7, 9, 11, and 12). Most harzburgites and lherzolites have protogranular textures, with recrystallization degrees variable from 10 to 30 vol%, and only one lherzolite (XML 3) grades into the porphyroclastic type. Reaction rims between xenolith and host basanite are not observed. Some peridotites contain intragranular or intergranular glass microveins which do not reach the contact with the host lava.

Olivine and orthopyroxene are present as strained porphyroclasts (4 - 25 mm in size) and smaller polygonal strain-free neoblasts (≤ 2 mm in size). Olivine porphyroclasts (Ol I) are

typically coarse-grained, with several grains up to 25 mm in size. Olivine porphyroclasts show kink-bands (Fig. 2b) and may contain trails of spinel inclusions. Orthopyroxene porphyroclasts (Opx I) have similar sizes. In less recrystallized protogranular harzburgites and lherzolites (about 10-20 vol% neoblasts), they show clinopyroxene ± spinel exsolution lamellae (Fig. 2c). In more recrystallized protogranular peridotites and in the porphyroclastic lherzolite, Opx I shows clear rims (Fig. 2d) or does not contain exsolution lamellae (Fig. 2e).

Olivine and orthopyroxene neoblasts (Ol II and Opx II) occur as interstitial grains or as aggregates of polygonal grains showing triple junctions. They are strain-free and can include minute spinel grains (Fig. 2f). In spinel dunites, Ol II grains are present distributed along preferred orientations, showing a rock foliation cutting large Ol I (Fig. 2h). Clinopyroxene and spinel have smaller sizes on average (1 mm) than Ol I and Opx I and occur both as subhedral and as interstitial grains. They may form symplectites with orthopyroxene and olivine (Fig. 2g).

In spinel harzburgites and lherzolites, olivine has a narrow Mg# (Mg# = ($Mg/Mg+Fe_{tot}$) ranging from 0.89 to 0.91, with slightly higher values in harzburgites. CaO content varies from 0.01 to 0.17 wt% and NiO from 0.31 to 0.48 wt%. No significant chemical variation between porphyroclasts and neoblasts has been observed, except for a higher CaO content, up to 0.17 wt%, in neoblasts. Opx I and Opx II also show similar and narrow Mg# interval, from 0.90 to 0.91. Al_2O_3 contents range from 2.1 to 3.7 wt%, Cr_2O_3 from 0.24 to 0.7 wt% and CaO from 0.36 to 0.81. TiO_2 content is very low (< 0.17 wt%). Clinopyroxene is Cr-diopside with Mg# ranging from 0.89 to 0.93. Cr_2O_3 varies from 0.48 to 1.1 wt%, Al_2O_3 ranges from 1.68 to 4.55 wt% and TiO_2 from 0 to 1.25 wt%. Spinel is a magnetite-spinel solid solution with a Cr# [Cr# = Cr/(Cr + Al)] variable from 0.25 to 0.35. Cr_2O_3 content ranges from 20.84 to 28.98 wt% and TiO_2 from 0 to 0.22 wt%. Chromite-rich rims (Cr# = 0.4 - 0.5) are observed in some grains.

238

239 Mineral geothermobarometry

240 Equilibration temperatures for peridotites were estimated considering the partitioning
241 of Fe^{2+}, Mg and Ca between orthopyroxene and clinopyroxene (Wells 1977; We), the two-
242 pyroxene and the Ca-in-opx thermometers (Brey and Koehler 1990; BK2px and BKopx), and
243 the solubility of Ca and Al in orthopyroxene in equilibrium with olivine, clinopyroxene and
244 spinel (Witt-Eickschen and Seck 1991; WS). Temperature estimates were performed in
245 exsolved porphyroclasts cores and clear porphyroclasts and neoblasts of harzburgites and
246 lherzolites.

247 Exsolved Opx I porphyroclasts provide equilibration temperatures comprised between
248 800 and 950°C. BK2px thermometer provides the lowest equilibration temperatures at 800°C,
249 while the We and BKopx thermometers give consistent temperatures, ranging from 800 to
250 920°C. WS thermometer provides the highest estimates, with temperatures reaching 950°C.
251 Clear Opx I thermometry yields higher temperatures, compared to the exsolved
252 porphyroclast thermometry, ranging from 900 to 1100°C. BK2px thermometer provides also
253 in this case the lower estimates with temperatures of approximately 900°C. We and BK opx
254 thermometers yield to more elevated T conditions, reaching 980°C. WS thermometer gives the
255 higher equilibration temperatures, from 950 to 1100°C. Temperatures estimates in neoblasts
256 show that peridotites from El Hierro have been locally heated to T > 1100°C (We and BK
257 thermometers).

258 From petrography and mineral geothermometry, it is possible to distinguish two groups
259 of peridotites: a first group is represented by harzburgites and lherzolites that present exsolved
260 Opx I porphyroclasts, which show equilibration temperature from 800 to 950°C (LT
261 peridotites; XML 7, 8, 10 and 11). A latter group corresponds to harzburgites and lherzolites

that contain clear Opx I porphyroclasts and higher equilibration temperatures from 900 to 1100°C (HT peridotites; XML 3, 4, 5 and 9). In peridotites from El Hierro and the other Canary Islands, a bimodal temperature distribution, in the same temperature intervals, was previously reported by Neumann et al. (2002; i.e., HEXO and HTR peridotites).

Pressures were estimated employing the Koehler and Brey (1990; KB) geobarometer, which considers the diffusion of calcium in olivine. The minimum equilibration pressures correspond to 1.5 GPa, while the maximum conditions reach pressures of 2 GPa. It has to be noted, however, that the KB barometer is strongly temperature dependent; consequently, pressure estimates have to be considered affected by a significant uncertainty.

Fluid inclusion study

Petrography of fluid inclusions

Nine representative samples of LT and HT peridotites were selected for fluid inclusion analysis. They consist of 3 dunites (XML 1, 5, and 10), 4 harzburgites (XML 4, 7, 9 and 11), and 2 lherzolites (XML3 and 9). Fluid inclusions are present in Ol I, Opx I and in clinopyroxene and are more abundant in LT peridotites. Neoblasts of Ol II and Opx II do not contain fluid inclusions.

Two main fluid inclusion assemblages (Roedder 1984; Bodnar 2003) have been recognized. Early Type I fluid inclusions are present only in Ol I and exsolved Opx I of LT peridotites (Fig. 3). Inclusions have rounded or negative-crystal shapes and sizes from ≤ 3 μm to 50 μm in length. They occur either in spatially isolated small clusters or as short

intragranular trails often along preferred crystallographic orientations (Fig. 3a-c). Type I inclusions are often associated with carbonate-rich inclusions and glass veins (Fig. 3b).

At room temperature, inclusions are CO_2-rich and single-phase (L; Fig. 3c), or they can contain several daughter minerals (i.e., carbonates, or carbonates + sulfates ± chlorides ± phosphates) and an opaque mineral (two-phase L+S inclusions; Fig., 3a, and d). The composition of daughter mineral phases has been determined by Raman microspectroscopy mapping (Fig. 4a). Carbonates are dolomite, or Mg-calcite and magnesite; sulfates include anhydrite, sulfohalite, and $MgSO_4*nH_2O$; phosphate is apatite; the opaque phase is either spinel, or magnetite, or hematite (Fig. 4 b-f).

The second fluid inclusion assemblage is represented by late Type II CO_2 fluid inclusions. Type II inclusions were trapped at later stages in Ol I, Opx I and clinopyroxene of both LT and HT peridotites. They occur as intragranular and intergranular trails of variable length and as isolated clusters (Fig. 5a, c). In exsolved Opx I, Type II inclusions are observed along preferential crystallographic orientations (e.g., 010; Fig. 5d). Inclusions have negative-crystal or rounded shapes and sizes ranging from less than 1 to 40 µm in length (Fig. 5b). At room temperature, they are single phase CO_2 (L) or, less commonly, two phase inclusions (L+V; Fig. 5) and do not contain daughter minerals. Decrepitation textures are frequently observed, particularly in HT peridotites (Fig. 5b and d).

Composition and density of fluid phases

The chemical composition and the density of Type I and II fluid inclusions have been determined by microthermometric and Raman microspectroscopic analyses. For those Type II inclusions with a size < 3µm, density has been calculated by the "Raman densimeter" (Kawakami et al. 2003).

Type I fluid inclusions.

Phase transitions have been observed in 15 single-phase (L) Type I inclusions of two LT peridotites in the temperature range from -190 to 20°C. On cooling, 14 inclusions freeze at temperatures variable from -95 to -80°C. On subsequent heating, inclusions show slow melting of solid CO_2, in a 2-3°C interval, with initial melting (Ti) recorded at about -60°C, and final melting (Tm) from -58.6 to -56.9 ± 0.1 °C (Fig. 6). Homogenization temperatures to the liquid phase (ThL) range from -52.0 to 8.0 ± 0.1°C. According to the classification of van den Kerkhof (1988), the recorded phase transitions (Ti; S+L→S+L+V, Tm; S+L+V→ L+V, ThL; SL+V→L) classify H3 type CO_2-rich inclusions containing minor additional gaseous species.

A single Type I inclusion (~ 10 μm in size, red arrow in Fig. 7a) shows a different microthermometric behavior. On cooling down to -190°C, solid CO_2 nucleation occurs in presence of a liquid and a vapor phase (L+S+V). On heating, four subsequent phase transitions are recorded. Partial homogenization in the presence of solid CO_2 (ThS; S+L+V→S+L) occurs at about -152°C; then, a small bubble re-appears at -95°C (Ti; S+L→S+L+V). On further heating, the partial homogenization in the presence of solid CO_2 (ThS; S+L+V→S+L) is measured at -61.0 ± 0.1°C. The last phase transition takes place by dissolution of solid CO_2 in a one-phase liquid-like fluid (Ts; S+L→L) at -60.0 ± 0.1°C. According to van den Kerkhof (1988), the observed sequence of phase transitions (S4 type fluid inclusions) identifies extremely dense CO_2-N_2 mixtures.

In all analyzed Type I inclusions, the presence of nitrogen has been confirmed by the N_2 band from 2228 to 2330 cm^{-1} in Raman spectra (Fig.7b and c). An N_2 molar fraction (X_{N2}) of 0.18 has been calculated for the S4-type CO_2-N_2 inclusion by quantitative Raman analysis (red arrow in Fig. 7a). H3-type inclusions contain less N_2, being X_{N2} comprised between 0.05

and 0.09 (Fig. 7a). The molar volume of CO_2-N_2 mixtures has been derived by plotting the measured sequence of phase transitions in the CO_2-N_2 T-X isochoric (cm^3/mole) diagram (Fig. 8) of van den Kerkhof (1988) and Klemd et al. (1992). For the S4-type inclusion (X_{N2} = 0.18 and Ths= -152°C) the corresponding molar volume is 34.5 cm^3/mol (i.e. d = 1.19 g/cm^3). For H3-type inclusions, molar volumes range from 38.5 cm^3/mole (X_{N2} = 0.05 - 0.09 and ThL from -52 to -51°C) to 40 - 50 cm^3/mole (X_{N2}= 0.01 and ThL from -35 to 8°C) (Figg. 7a and 8).

Type II fluid inclusions.

On cooling, Type II CO_2 fluid inclusions freeze at temperatures variable from -95 to -65°C. Solid CO_2 melts instantaneously from -57.3 to -56.5 ± 0.1°C (Tm; n=50), with most measurements at -56.6 °C (Fig. 6). Melting behavior indicates that fluid inclusions consist of pure CO_2, as confirmed by Raman analysis. Liquid water and/or clathrates have not been observed in any of the measured inclusions by both analytical techniques.

Type II pure CO_2 inclusion homogenization occurs to the liquid phase (ThL; n = 512) with a scattered distribution from -37.5 to 31.0 ±0.1°C (Fig. 9). Only the 2% of analyzed inclusions has homogenization to the vapor phase (not shown). Interestingly, when ThL values are plotted separately for inclusions in LT and HT peridotites, measurements define two frequency intervals at slightly different temperatures (Fig. 10). In LT peridotites, the two frequency intervals range from -37.5 to -12°C and from 20 to 31°C, respectively (Fig. 10a). In HT peridotites, the first ThL distribution interval occurs at slightly higher temperatures, from -24 to 0°C, while the latter occurs in the same interval from 20 to 31 °C (Fig. 10b). Corresponding CO_2 density values range between 1.11 and 1 ± 0.01 g/cm^3 and 0.75 and 0.65 ± 0.01 g/cm^3 in LT peridotites, and between 1.04 and 0.91 ± 0.01 g/cm^3 and 0.75 and 0.65 ± 0.01 g/cm^3 in HT peridotites.

As a general rule of thumb, the preservation of fluid inclusion depends on both inclusion size and on the mechanical properties of the enclosing mineral (e.g. Bodnar et al. 1989; Campione et al. 2015). For this reason, the distribution of ThL measurements for Type II CO_2 inclusions has also been investigated in the different mineral phases. As shown by the histograms in Figure 11, ThL distribution is similar in orthopyroxene and clinopyroxene where the lowest ThL values correspond to a density of 1.11 ± 0.1 g/cm^3. Conversely, in olivine, ThL's are systematically higher, resulting in lower CO_2 densities not exceeding 1 ± 0.1 g/cm^3. Therefore, measured Type II inclusions in olivine have not preserved fluid density at trapping P-T conditions.

To test if partial decrepitation and/or stretching in olivine was dependent on inclusion size, the densities of 37 inclusions with length ≤ 3 μm have been calculated by applying the Raman densimeter of Kawakami et al. (2003). In Raman spectra, measured distances of the CO_2 Fermi doublet (Δ) from 105.17 to 104.46 ± 0.03 cm^{-1} correspond to CO_2 densities between 1.11 to 0.85 ± 0.1 g/cm^3 (Fig. 12a). This density interval is similar to that obtained by microthermometry in larger CO_2 inclusions in orthopyroxene and clinopyroxene (Fig. 12a). Thus, data indicate a greater tendency to decrepitation of fluid inclusions in olivine than in pyroxenes, probably due to mechanical failure on decompression from mantle depths.

Discussion

Significance of fluid inclusion data

In mantle xenoliths, fluid inclusions represent either mantle metasomatic fluids, or fluids degassed by ascending basaltic magmas (cf., Andersen and Neumann 2001; Frezzotti

and Touret 2014, and references therein). The chemical composition and the density of metasomatic and magmatic fluids can be different, since trapping can occurs at various pressure and temperature conditions. Therefore, the chemical composition and the density distribution of fluid inclusions potentially provide plentiful information on the depths of origin of mantle rocks, and/or on the episodes of rest magma at confined depths (c.f., Andersen and Neumann 2001; Frezzotti and Peccerillo 2004; Hansteen and Klügel 2008).

The reliability of fluid inclusions as geobarometers relies on the isochoric principle, governed by the fluid equation of state (Roedder 1965). At trapping P-T conditions, the pressure of the fluid inside the inclusions equals the lithostatic pressure. During magma transport, however, the fluid develops relevant overpressures, since the external lithostatic or magmatic pressure becomes progressively lower than the internal fluid pressure (Roedder 1984). If fluid overpressure exceeds the mechanical strength of the enclosing mineral, fluid inclusions undergo decrepitation and stretching, with a partial-to-complete fluid loss, resulting in a density decrease. Inclusion decrepitation and stretching depend on many variables, such as the composition, size and distribution of the fluid inclusions, and the mechanical strength of the host mineral (e.g., Bodnar et al. 1989; Vityk and Bodnar 1998; Frezzotti and Viti 2001; Campione et al. 2015), but it does not reflect a decrease in magma decompression rates. A slowing down of the ascent rate of magmas - which corresponds to magma rest episodes at confined depths - can be proposed if decrepitation and stretching reset inclusion densities to newly-defined lower-pressure intervals and new episodes of fluid trapping occur (cf., Andersen and Neumann 2001; Frezzotti and Peccerillo 2004; Hansteen and Klügel 2008).

The present study reveals trapping of fluids during subsequent events. Type I inclusions represent the earlier and deeper fluids, as indicated by their distribution as small clusters or as crystallographically oriented groups in Ol I and exsolved Opx I of LT peridotites. Type I fluids are CO_2-rich and contain variable amounts of N_2, reaching 18 mol%

403 in the densest inclusion (1.19 g/cm^3). Their association with CO_2-N_2 inclusions containing
404 carbonates, sulfates, ± chlorides and spinel, and with carbonate-silicate glass micro-veins
405 suggest an origin by immiscibility processes from an original volatile-rich carbonate-silicate
406 melt in the lithospheric mantle.

407 In the Canary Islands, mantle metasomatism by carbonatitic or carbonate-silicate
408 melts, enriched in volatiles and incompatible trace elements, was previously described. In
409 particular, carbonate-rich hydrous fluids or melts were reported in peridotites from Tenerife,
410 Lanzarote, and La Gomera (Frezzotti et al. 2002a, b; Neumann et al. 1995; 2002; 2004).
411 Likewise, N_2 in CO_2 mantle fluids was reported in peridotites from Lanzarote (Andersen et al.
412 1995). Notably, the presence of N_2 in CO_2-rich inclusions was also in this case revealed by
413 Raman microspectroscopy, being Raman the only analytical technique able to detect trace
414 amounts (≤ 0.1 mol%) of N_2 in fluid inclusions of small size. Metasomatic processes predate
415 the onset of Canary magmatism (Neumann et al. 2004) and are unrelated to the ascent history
416 of peridotites in the host lavas.

417 At a later stage, ingression of lower-density CO_2 fluids occurred in both LT and HT
418 peridotites. Type II inclusion distribution along intergranular trails is suggestive of fluid
419 trapping by micro-fracturing of peridotites. CO_2 density distribution intervals suggest two
420 distinct fluid trapping and re-equilibration events (Fig. 10). In LT peridotites (T = 800 -
421 950°C), density intervals are from 1.11 to 0.99 ± 0.01 g/cm^3 and from 0.75 to 0.65 ± 0.01
422 g/cm^3, respectively (Fig. 12a). In peridotites equilibrated at higher temperatures (HT
423 peridotites; T = 900-1100 °C), CO_2 density distribution shows similar, although slightly lower,
424 values from 1.04 to 0.91 ± 0.01 g/cm^3 and from 0.75 to 0.65 ± 0.01 g/cm^3, respectively (Fig.
425 12b).

426 The clear-cut variation of the chemistry of Type II inclusions, which consist of pure
427 CO_2, suggests a different fluid origin, probably by degassing of magmas. Canary alkaline
428 mafic magmas are carbon-rich and thus can begin to exsolve CO_2-rich fluids at great pressures
429 (> 1 GPa; Longpré et al. 2017) in the oceanic lithospheric mantle.

430

431 Fluid inclusions geothermobarometry

432 Once the composition and density of the fluids are defined, temperatures be known in
433 order to calculate pressure conditions by fluid equations of state (Roedder 1965; 1984). In
434 general, the temperature of the host lavas is taken as representative of fluid trapping conditions
435 in mantle xenoliths (cf., Andersen and Neumann 2001; Hansteen and Klügel 2008). In the
436 present case, however, the preservation of Type I inclusions only in LT peridotites, and the
437 density differences of Type II CO_2 fluids in LT and HT peridotites suggest that xenoliths did
438 not reach the same temperatures during ascent. For this reason, fluid trapping temperatures
439 have been assumed based on mantle mineral geothermometry: 800 - 950°C for LT peridotites,
440 and 900 - 1100°C for HT peridotites (Wells 1977, Brey and Koehler 1990 and Witt-Eickschen
441 and Seck 1991). From each temperature interval, the highest value has been selected assuming
442 the presence of a component of increasing temperature caused by the ascent of mantle
443 xenoliths in the basaltic host lavas.

444 The P-T distribution of Type I and II fluid isochores is reported in Figure 13. The
445 extremely high densities of Type I CO_2-N_2 fluids in LT peridotites (1.19 g/cm^3; inclusion S4),
446 correspond to trapping pressures of 1.8 ± 0.02 GPa at 950°C (gray star in Fig. 13). This
447 pressure is consistent with mineral geobarometry data, which indicate equilibration of
448 peridotites in the mantle at 1.5 - 2.0 GPa for the same temperatures (Koehler and Brey 1990).

449 Conversely, trapping and/or re-equilibration of Type II CO_2 fluids occurred at lower
450 pressures (Fig. 13) during two distinct episodes of magma rest at confined depths. In LT
451 peridotites, isochore distribution for the denser Type II inclusions correspond to pressures
452 comprised from 1 to 0.67 ± 0.02 GPa, at 950°C (green band in Fig. 13). In HT peridotites,
453 Type II fluid isochores indicate similar, though slightly lower, pressures from 0.89 to 0.60 ±
454 0.02 GPa at 1100 °C (blue band in Fig. 13). As illustrated in the P-T diagram in Figure 13,
455 largely overlapping isochoric bands confirm that Type II inclusions in both LT and HT
456 peridotites record a common deep magma storage region. The somewhat higher pressure
457 values calculated for Type II fluids in LT rocks (Fig. 13) put forward that fluid inclusions are
458 better preserved in rocks equilibrated at lower temperatures.

459 A second CO_2 trapping and re-equilibration event is defined by isochoric pressures
460 (red isochore bands in Fig. 13) from 0.34 to 0.26 ± 0.02 GPa at 950°C (Type II inclusions in
461 LT peridotites) and from 0.36 to 0.28 ± 0.02 GPa at 1100°C (Type II inclusions in HT
462 peridotites). In HT and LT peridotites, the isochore bands for Type II inclusions differ from
463 each other of only 0.02 GPa. This negligible pressure variation confirms the accuracy of
464 pressure estimates. This fluid trapping event corresponds to the last episode of magma rest
465 before eruption.

466

467 Recent magma transport dynamics beneath El Hierro

468 In order to model magma transport dynamics beneath El Hierro, once having found the
469 P-T conditions for fluid trapping, we have to define the corresponding depths. Fluid isochoric
470 pressures have been converted into depths following the relation: h= P/(g*d), where h is the
471 depth of origin or trapping of the fluids, P the lithostatic pressure, g the acceleration of gravity
472 (9.81 m/sec^2), and d the density of column-rocks. Main rock layer densities have been defined

473 based on the following simplified stratigraphic reconstruction: a sequence of volcanic products
474 and rocks with a density of 2.5 g/cm^3 for the volcanic edifice (emergent and submarine height
475 of island of about 4500 m; Acosta et al. 2005; Carracedo et al. 2012), a basaltic oceanic crust
476 with a density of 2.7 g/cm^3 (about 8500 m), and lithospheric peridotites with a density of 3.3
477 g/cm^3.

478 Fluid inclusions studies in peridotite xenoliths allow concluding that polybaric magma
479 transport characterizes the Rift Volcanism activity at about 40-30 ka. The resulting model is
480 illustrated schematically in Figure 14 and discussed in the following sections.

481 El Hierro volcano is built on oceanic crust extending to about 12 - 15 km (Martinez et
482 al. 2013) of a thick lithosphere of about 90 - 95 km (Dasgupta et al. 2010). Type I CO_2-N_2
483 fluids associated with carbonate-silicate melts indicate that peridotites erupted from a source
484 within the depth range of 60-65 km ($P = 1.80 \pm 0.02$ GPa; gray star in Fig. 14) in the lower
485 lithospheric mantle. As discussed in the previous sections, geochemical characteristics of
486 peridotites beneath the Canary islands point to mantle metasomatism by carbonate-rich melts
487 (e.g. Neumann 2004). The presence of oceanic carbonatites of Oligocene to Lower Miocene
488 age in Fuerteventura (Lebas et al. 1986) provides further support to a carbonate enriched
489 lithosphere.

490 Type II fluid inclusions have been trapped during magma rest at confined depths for a
491 time sufficient to allow CO_2 trapping. Fluid density distribution identifies two main magma
492 accumulation regions. The deeper one is located in the shallow lithospheric mantle at depths
493 comprised from 37 to 22 km (Fig. 14). This mantle magma reservoir served as the main
494 storage volume of the volcano and fed a smaller reservoir at 10 - 12 km depth (Fig. 14) near
495 the base of the oceanic crust, from where mafic magmas erupted.

Magma storage at crustal conditions does not appear to be long-lived. The preservation of high-density Type I and II inclusions suggests that mafic magmas arrived into the lower oceanic crust shortly before (e.g. day timescale) the eruption. Longer magma stagnation would have caused the complete resetting of fluid inclusion densities to shallower ambient pressures (Wanamaker and Evans 1989; Hansteen and Klügel 2008).

The lithospheric mantle reservoir revealed by present study is particularly thick, on the order of 15 km (i.e. from 37 to 22 km depth). Thus, magma is likely to have been stored in a series of interconnected pockets distributed over this wide depth interval (Fig. 14). Similar magma accumulation as vertically-stacked small reservoirs has been previously characterized for Kilauea and Piton de la Fournaise (Decker 1987; Ryan et al. 1988; Voogd et al. 1999; Michon et al. 2015). In these volcanoes, deep magma transport dynamics has been interpreted as the result of magma storage in the lithospheric mantle, either through a micro-fracture network system over a wide depth interval (e.g. magma-fracking by CO_2 degassing; Shaw et al. 1980; Pollard et al. 1983; Decker 1987), or in a porous mantle matrix (Gudmundsson 1987). Partially molten mantle storage regions where magma rest and degas are considered to be long-lived (Shaw et al. 1980; Pollard et al. 1983; Decker 1987); although their formation is still not unanimously accepted, they have been proposed in regions of oceanic intraplate volcanism characterized by slow magma supply (e.g. Shaw et al. 1980), which would be in agreement with the low long-term magma rate of El Hierro volcano (0.12-0.13 km^3/ka; Carracedo 1999).

The proposed polybaric magma storage system appears to agree with magma transport dynamics reconstructed for the 2011-2012 eruption (e.g., Meletlidis et al. 2012; Becerill et al. 2013b; González et al., 2013; Martí et al. 2013; Longpré et al. 2014; Klügel et al. 2015). Therefore, it seems that the magma plumbing system has been essentially the same for the last 30–40 ka. For instance, the upper limit of the deep magma storage region identified by fluid

inclusions at approximately 22 km (Fig. 14) corresponds to the depth of the pre- sin-eruptive earthquake hypocenters (20 - 25 km) interpreted to reflect the magma source that fed the 2011-2012 eruption (e.g. López et al. 2012; Martí et al. 2013; Longpré et al. 2014). Furthermore, storage of 2011-2012 magma in the lower oceanic crust is likewise considered ephemeral, not developing into a long-term reservoir (e.g., Becceril et al. 2013b; Longpré et al. 2014; Martí et al. 2013; Klügel et al. 2015). These Authors further interpreted the pre-eruptive lateral magma migration of about 15–20 km from north to south as evidence of sill propagation. Although fluid inclusion data cannot resolve horizontal magma movements, temporary magma stagnation in a region of neutral buoyancy, such as the lower crust, might have favored lateral transport.

In oceanic islands, magma pathways are established in the early growth stages but evolve on time, along with the volcano. Our model does not indicate storage of magmas directly beneath the Moho (i.e., 15 to 25 km) for present rift volcanism activity, as previously proposed by Stroncik et al. (2009) based on clinopyroxene-melt geobarometric data in prehistorical lavas of undetermined age. Confinement of magmas at about 7-10 km below the geophysical interface of the oceanic crust and the mantle (12 - 15 km; Fig. 14) can be tentatively interpreted as an indication of magma underplating below El Hierro. At the nearby island of La Palma, progressive deepening of the magma plumbing system, induced by up to 10 km magma underplating, has been recently proposed by Barker et al. (2015). Similarly, geophysical data from the Canary Islands (Carracedo et al. 2015) point to underplating beneath Tenerife and Gran Canaria over the same depth interval. In this respect, further studies of fluid inclusions in mantle xenoliths in lavas of older volcanic cycles of El Hierro should make it possible to trace the evolution of magma transport beneath this volcano over its entire history.

Summary and Conclusions

Present study focuses on the reconstruction of a model for the recent magma dynamics beneath El Hierro Island based on combined fluid inclusion and mineral geothermobarometry in mantle xenoliths entrained in lavas of the Rift Volcanism activity (40-30 ka). Two distinct fluid phases have been characterized by microthermometry and Raman microspectroscopy. Type I CO_2-N_2 mantle metasomatic fluids are trapped at pressure of 1.80 ± 0.02 GPa, or about 60-65 km depth, before xenolith entrainment in the host lava. Type II CO_2 fluids, probably degassed from host mafic magmas, reveal two discrete magma accumulation regions: the first in the lithospheric mantle, from 1 to 0.60 ± 0.02 GPa, or 37 to 22 km depth, and the latter in the lower oceanic crust, from 0.34 to 0.21± 0.02 GPa, or 12 to 10 km depth,. The deeper accumulation region is interpreted as a staked system of interconnected small magma pockets distributed in the lithospheric mantle beneath the Island, which fed a temporary lower crustal storage region.

Models of the internal structure of active volcanoes are important for constraining reliable monitoring strategies and forecasting volcanic eruptions. Present fluid inclusion study can probably produce a reliable model on how El Hierro volcano works, since magma migration within the plumbing system is comparable to that registered during the 2011-2012 eruption. The implications are that magma migration from the deep reservoir should be monitored as precursor of magma rise and hence eruption, by considering both mantle seismicity, conceivably connected with upward migration of earthquake hypocenters, and changes in the gravity field as a consequence of magma migration within the plumbing system.

570 **Acknowledgements**

571

572 This paper is a part of E.O. Ph.D. thesis. We are grateful to L. Becceril, M. Campione,
573 F. Lucchi, N. Malaspina, and V. Zanon for helpful discussions. We acknowledge A.
574 Risplendente for assistance during microprobe analyses. Editorial handling by V. Kamenetsky,
575 and reviews by F. Deegan, T. Hansteen and an anonymous reviewer have considerably
576 improved the manuscript. Funding was provided by the University of Milan Bicocca, FAR-
577 2015 to M.L.F and I.M.V.. Raman facilities were provided by the Interdepartmental Center
578 "G. Scansetti" for studies on asbestos and other toxic particulates at the University of Turin.

579

580

581

582 **References**

583

584 Acosta J, Uchupi E, Muñoz A, Herranz P, Palomo C, Ballesteros M, Working ZE (2005)
585 Geologic evolution of the Canarian Islands of Lanzarote, Fuerteventura, Gran Canaria and
586 La Gomera and comparison of landslides at these islands with those at Tenerife, La Palma
587 and El Hierro. Mar Geophys Res 24:1–40

588 Andersen T, Burke EJ, Neumann ER (1995) Nitrogen-rich fluid in the upper mantle: fluid
589 inclusions in spinel dunite from Lanzarote, Canary Islands. Contrib Mineral Petrol
590 120:20–28

591 Andersen T, Neumann ER (2001) Fluid inclusions in mantle xenoliths. Lithos 55:301–32.

592 Anguita F, Hernan F (1975) A propagating fracture model versus a hot spot origin for the
593 Canary Islands. Earth Planet Sci Lett 27:11–19

594 Anguita F, Hernán F (2000) The Canary Islands origin: a unifying model. J Volcanol and
595 Geotherm Res 103:1–26. http://doi/10.1016/S0377- 0273(00)00195- 5

596 Araña V, Ortiz R (1991) The Canary Islands: tectonics, magmatism and geodynamic
597 framework. In: A. Kampunzu, R. Lubala (eds) Magmatism in Extensional Structures
598 Setting: The Phanerozoic African Plate, Springer Verlag, pp. 209–249

599 Bakker RJ (2003) PackageFLUIDS1. Computer programs for analysis of fluid inclusion data
600 and for modelling bulk fluid properties. Chem Geol 194:3–23

601 Barker AK, Troll VR, Carracedo JC, Nicholls PA (2015) The magma plumbing system for the
602 1971 Teneguía eruption on La Palma, Canary Islands. Contrib Mineral Petrol 170:5–6

603 Becerril L, Cappello A, Galindo I, Neri M, Del Negro C (2013a) Spatial probability
604 distribution of future volcanic eruptions at El Hierro Island (Canary Islands, Spain). J
605 Volcanol Geotherm Res 257:21–30

606 Becerril L, Galindo I, Gudmundsson A, Morales JM (2013b) Depth of origin of magma in
607 eruptions. Sci Rep 3:1–6. http://doi.org/10.1038/srep02762

608 Becerril L, Galindo I, Martí J, Gudmundsson A (2015) Three-armed rifts or masked radial
609 pattern of eruptive fissures? The intriguing case of El Hierro volcano (Canary Islands).
610 Tectonophysics 647:33–47

611 Bertagnini A, Métrich N, Landi P, Rosi M (2003) Stromboli volcano (Aeolian Archipelago,
612 Italy): an open window on the deep-feeding system of a steady state basaltic volcano. J
613 Geophys Res 108: 2336-2342

614 Bodnar RJ (2003) Introduction to aqueous-electrolyte fluid inclusions. Fluid Inclusions:
615 Analysis and Interpretation. In I. Samson, A. Anderson, D. Marshall (eds) Mineral Assoc
616 Canada, Short Course 32, pp. 81-100

617 Bodnar RJ, Binns PR, Hall DL (1989) Synthetic fluid inclusions-VI. Quantitative evaluation
618 of the decrepitation behaviour of fluid inclusions in quartz at one atmosphere confining
619 pressure. J Metam Geol 7:229–242

620 Brey GP, Köhler T (1990) Geothermobarometry in four-phase lherzolites II. New
621 thermobarometers, and practical assessment of existing thermobarometers. J Petrol
622 31:1353–1378

623 Campione M, Malaspina N, Frezzotti ML (2015) Threshold size for fluid inclusion
624 decrepitation. J Geophys Res Solid Earth 120:7396–7402

625 Carracedo JC (1994). The Canary Islands: an example of structural control on the growth of
626 large ocean-island volcanoes. J Volcanol Geotherm Res 60:225–241

627 Carracedo JC (1999) Growth, structure, instability and collapse of Canarian volcanoes and
628 comparisons with Hawaiian volcanoes. J Volcanol Geotherm Res 94:1–19

629 Carracedo JC, Day S, Guillou H, Rodríguez Badiola E, Canas JA, Pérez Torrado FJ (1998)
630 Hotspot volcanism close to a passive continental margin: the Canary Islands. Geol Mag
631 135: 591–604

632 Carracedo JC, Badiola ER, Guillou H, de La Nuez J, Pérez Torrado FJ (2001) Geology and
633 volcanology of La Palma and El Hierro (Canary Islands). Estudios Geol 57:175–273

634 Carracedo JC, Perez-Torrado FJ, Rodriguez-Gonzalez A, Fernandez-Turiel JL, Klügel A,
635 Troll, VR, Wiesmaier S (2012) The ongoing volcanic eruption of El Hierro, Canary
636 Islands. Eos 93: 89–90

637 Carracedo JC., Troll VR, Zaczek K, Rodriguez-Gonzalez A, Soler V, Deegan FM (2015) The
638 2011–2012 submarine eruption off El Hierro, Canary Islands: New lessons in oceanic
639 island growth and volcanic crisis management. Earth-Sci Rev 150:168–200

640 Dasgupta R, Jackson MG, Lee C-TA (2010) Major element chemistry of ocean island basalts -
641 Conditions of mantle melting and heterogeneity of mantle source. Earth Planet Sci Lett
642 289:377–392

643 De Vivo B, Frezzotti ML, Lima A, Trigila R (1988) Spinel lherzolite nodules from Oahu
644 Island (Hawaii): a fluid inclusion study. Bull Mineral 111:307–319

645 Decker RW, Wright TL, Stauffer, S (1987). Volcanism in Hawaii. US Government Printing
646 Office, p 1606

647 Duggen S, Hoernle K, Hauff F, Klügel, A, Bouabdellah M, Thirlwall MF (2009) Flow of
648 Canary mantle plume material through a subcontinental lithospheric corridor beneath
649 Africa to the Mediterranean. Geology 37:283–286

650 Duschek W, Kleinrahm R, Wagner W (1990) Measurement and correlation of the (pressure,
651 density, temperature) relation of carbon dioxide I. The homogeneous gas and liquid
652 regions in the temperature range from 217 K to 340 K at pressures up to 9 MPa. J Chem
653 Thermod 22:827–840. http://doi.org/10.1016/0021-9614(90)90172-M

654 Frey FA, Prinz M (1978) Ultramafic inclusions from San Carlos, Arizona: petrologic and
655 geochemical data bearing on their petrogenesis. Earth Planet Sci Lett 38:129–176

656 Frezzotti ML, Peccerillo A (2004) Fluid inclusion and petrological studies elucidate
657 reconstruction of magma conduits. Eos 85:157–160

658 Frezzotti ML, Touret JL (2014) CO_2, carbonate-rich melts, and brines in the mantle. Geosci
659 Front 5:697-710

660 Frezzotti ML, De Vivo B, Clocchiatti R (1991) Melt-mineral-fluid interactions in ultramafic
661 nodules from alkaline lavas of Mount Etna (Sicily, Italy): melt and fluid inclusion
662 evidence. J Volcanol Geotherm Res 47:209–219

663 Frezzotti ML, Touret JL, Lustenhouwer WJ, Neumann ER (1994) Melt and fluid inclusions in
664 dunite xenoliths from La Gomera, Canary Islands: tracking the mantle metasomatic fluids.
665 Eur J Mineral 6:805–817

666 Frezzotti ML, Andersen T, Neumann ER, Simonsen SL (2002a) Carbonatite melt–CO_2 fluid
667 inclusions in mantle xenoliths from Tenerife, Canary Islands: a story of trapping,
668 immiscibility and fluid–rock interaction in the upper mantle. Lithos 64:77–96

669 Frezzotti ML, Touret JL, Neumann ER (2002b) Ephemeral carbonate melts in the upper
670 mantle. Eur J Mineral 14:891–904

671 Frezzotti ML, Tecce F, Casagli A (2012) Raman spectroscopy for fluid inclusion analysis. J
672 Geochem Explor 112:1–20

673 Füster J (1975) Las Islas Canarias: un ejemplo de evolución temporal y espacial del
674 vulcanismo oceánico. Est Geol 31: 439–463

675 Garrabos Y, Tufeu R, Le Neindre B, Zalczer G, Beysens D (1980) Rayleigh and Raman
676 scattering near the critical point of carbon dioxide. J Chem Phys 72:4637–4651

677 Gee MJR, Masson DG, Watts AB, Mitchell NC (2001) Offshore continuation of volcanic rift
678 zones, El Hierro, Canary Islands. J Volcanol Geother Res 105:107–119

679 Geyer A, Martí J (2010) Tectonophysics The distribution of basaltic volcanism on Tenerife,
680 Canary Islands: Implications on the origin and dynamics of the rift systems.
681 Tectonophysics 483: 310–326

682 González PJ, Samsonov SV, Pepe S, Tiampo KF, Tizzani P, Casu F, Sansosti E (2013)
683 Magma storage and migration associated with the 2011 – 2012 El Hierro eruption:
684 Implications for crustal magmatic systems at oceanic island volcanoes, J Geophys Res
685 Solid Earth 118:4361–4377

686 Gudmundsson A (1987) Geometry, formation and development of tectonic fractures on the
687 Reykjanes Peninsula, southwest Iceland. Tectonophysics 139: 295–308

688 Guillou H, Carracedo JC, Torrado FP, Badiola ER (1996) K-Ar ages and magnetic
689 stratigraphy of a hotspot-induced, fast grown oceanic island: El Hierro, Canary Islands. J
690 Volcanol Geother Res 73:141–155

691 Hansteen TH, Klügel A, (2008) Fluid inclusion thermobarometry as a tracer for magmatic
692 processes. In: Putirka KD, Tepley FJ (eds) Reviews in Mineralogy Min Soc Amer
693 149:143–177

694 Hansteen TH, Andersen T, Neumann ER, Jelsma H (1991) Fluid and silicate glass inclusions
695 in ultramafic and mafic xenoliths from Hierro, Canary Islands: implications for mantle
696 metasomatism. Contrib Mineral Petrol 107:242–254

697 Hansteen TH, Klügel A, Schmincke HU (1998) Multi-stage magma ascent beneath the Canary
698 Islands: evidence from fluid inclusions. Contrib Mineral Petrol 132:48–64

699 Hoernle K, Schmincke HU (1993) The Role of Partial Melting in the 15-Ma Geochemical
700 Evolution of Gran Canaria: A Blob Model for the Canary Hotspot, J Petrol 34:599–626

701 Hoernle KAJ (1998) Geochemistry of Jurassic oceanic crust beneath Gran Canaria (Canary
702 Islands): implications for crustal recycling and assimilation. J Petrol 39:859–880

703 Holloway JR (1977). Fugacity and activity of molecular species in supercritical fluids. In: DG
704 Fraser (ed) in Thermodynamics in Geology, Dordrecht-Holland, pp. 161–181

705 Holloway JR (1981) Compositions and volumes of supercritical fluids. In: L Hollister, ML
706 Crawford (eds) Fluid inclusions: application to petrology, Short Course Handbook, pp. 13-
707 38

708 IGME (2010a) Mapa Geológico de España, Escala 1:25.000. Isla de El Hierro. Hoja 1105- II,
709 Valverde, pp, 96

710 IGME (2010b) Mapa Geológico de España, Escala 1:25.000. Isla de El Hierro. Hoja 1105- III,
711 Sabinosa, pp, 71

712 IGME (2010c) Mapa Geológico de España, Escala 1:25.000. Isla de El Hierro. Hoja 1105- IV,
713 Frontera, pp, 84

IGME (2010d) Mapa Geológico de España, Escala 1:25.000. Isla de El Hierro. Hoja 1108-I/II, La Restinga, pp, 55

Kawakami Y, Yamamoto J, Kagi H (2003) Micro-Raman Densimeter for CO_2 Inclusions in Mantle-Derived Minerals. Applied Spectrosc 57:1333–1339

Klemd R, van den Kerkhof, AM, Horn EE (1992) High-density $CO_2 - N_2$ inclusions in eclogite-facies metasediments of the Münchberg gneiss complex, SE Germany. Contrib Mineral Petrol 111:409–419

Klügel A, Hansteen TH, Galipp K (2005) Magma storage and underplating beneath Cumbre Vieja volcano, La Palma (Canary Islands). Earth Planet Sci Lett 236:211–226

Klügel A, Longpré MA, García-Cañada L, Stix J, (2015) Deep intrusions, lateral magma transport and related uplift at ocean island volcanoes. Earth Planet Sci Lett 43:140–149

Koehler TP, Brey GP, (1990) Calcium exchange between olivine and clinopyroxene calibrated as a geothermobarometer for natural peridotites from 2 to 60 kb with applications. Geochim Cosmochim Acta 54:2375–2388

Lebas MJ, Rex DC, Stillman CJ (1986) The early magmatic chronology of Fuerteventura, Canary Islands. Geol Mag 123: 287–298

Longpré MA, Chadwick JP, Wijbrans J, Iping R (2011) Age of the El Golfo debris avalanche, El Hierro (Canary Islands): New constraints from laser and furnace 40Ar/ 39Ar dating. J Volcanol Geother Res 203:76–80

Longpré MA, Klügel A, Diehl A, Stix J (2014) Mixing in mantle magma reservoirs prior to and during the 2011 – 2012 eruption at El Hierro, Canary Islands. Geology 42:315–318

Longpré MA, Stix J, Klügel A, Shimizu N (2017) Mantle to surface degassing of carbon-and sulphur-rich alkaline magma at El Hierro, Canary Islands. Earth Planet Sci Lett 460:268-280

López C, Blanco MJ, Abella R, Brenes B, Cabrera Rodríguez VM, Casas B, Domínguez Cerdeña I, Felpeto A, Fernández de Villalta M, del Fresno C, García O, García-Arias MJ, García-Cañada L, Gomis Moreno A, González-Alonso E, Guzmán Pérez J, Iribarren F, López-Díaz R, Luengo-Oroz N, Meletlidis S, Moreno M, Moure D, Pereda de Pablo J, Rodero E, Romero E, Sainz-Maza S, Sentre Domingo MA, Torres PA, Trigo, P, Villasante-Marcos V (2012) Monitoring the volcanic unrest of El Hierro (Canary Islands) before the onset of the 2011–2012 submarine eruption. Geophys Res Lett 39 L13303

Lustrino M, Wilson M (2007) The circum-Mediterranean anorogenic Cenozoic igneous province: Earth-Sci Rev 81: 1–65

Marinoni LB, Pasquaré G (1994) Tectonic evolution of the emergent part of a volcanic ocean island: Lanzarote, Canary Islands. Tectonophysics 239:111–137

Marinoni LB, Gudmundsson A (2000) Dykes, faults and palaeostresses in the Teno and Anaga massifs of Tenerife (Canary Islands). J Volcanol and Geother Res 103:83–103

Martí J, Pinel V, Lõpez C, Geyer A, Abella R, Tárraga M, Rodríguez C (2013a) Causes and mechanisms of the 2011-2012 El Hierro (Canary Islands) submarine eruption. J Geophy Res Solid Earth, 118:823–839

Martí J, Castro A, Rodríguez C, Costa F, Carrasquilla S, Pedreira R, Bolos X (2013b) Correlation of magma evolution and geophysical monitoring during the 2011-2012 El Hierro (Canary Islands) submarine eruption. J Petrol 54:1349–1373

Martinez-Arevalo C, Mancilla FD, Helffrich G, Garcia A (2013) Seismic evidence of a regional sublithospheric low velocity layer beneath the Canary Islands. Tectonophysics 608:586–599

Masson DG (1996) Catastrophic collapse of the volcanic island of Hierro 15 ka ago and the history of landslides in the Canary Islands. Geology 24: 231–234

Masson DG, Watts B, Gee MJR, Urgeles R, Mitchell NC, Le Bas TP, Canals M. (2002) Slope failures on the flanks of the western Canary Islands. Earth-Sci Rev 57:1–35

Masson DG, Harbitz CB, Wynn RB, Pedersen G, Løvholt F (2006) Submarine landslides: processes, triggers and hazard prediction. Philosophical Transactions. Series A Math Physical Eng Sci 364:2009–2039

Meletlidis S, Roberto A, Di Pompilio M, Bertagnini A, Iribarren I, Felpeto A, Oriano CD (2012) Xenopumices from the 2011 – 2012 submarine eruption of El Hierro (Canary Islands, Spain): Constraints on the plumbing system and magma ascent, Geophy Res Lett 39:1–6

Michon L, Ferrazzini V, Di Muro A, Villeneuve N, Famin V (2015) Rift zones and magma plumbing system of Piton de la Fournaise volcano: How do they differ from Hawaii and Etna? J Volcanol Geother Res 303:112–129

Morgan DJ, Jerram DA, Chertkoff DG, Davidson JP, Pearson DG, Kronz A, Nowell GM (2007) Combining CSD and isotopic microanalysis: Magma supply and mixing processes at Stromboli Volcano, Aeolian Islands, Italy. Earth Planet Sci Lett 260:419–431

Neumann E (1990) Ultramafic and mafic xenoliths from Hierro, Canary Islands: evidence for melt infiltration in the upper mantle. J Chem 53:1689–1699

Neumann ER, Wulff-Pedersen E, Johnsen K, Andersen T, Krogh E (1995) Petrogenesis of spinel harzburgite and dunite suite xenoliths from Lanzarote, eastern Canary Islands: Implications for the upper mantle. Lithos 35:83–107

Neumann ER, Wulff-Pedersen E, Pearson NJ, Spencer EA (2002) Mantle Xenoliths from Tenerife (Canary Islands): Evidence for Reactions between Mantle Peridotites and Silicic Carbonatite Melts inducing Ca Metasomatism. J Petrol 43:825–857

Neumann ER, Griffin WL, Pearson NJ, O'Reilly SY (2004) The evolution of the upper mantle beneath the Canary Islands: Information from trace elements and Sr isotope ratios in minerals in mantle xenoliths. J Petrol 45: 2573–2612

Pasteris JD, Wopenka B, Seitz JC (1988) Practical aspects of quantitative laser Raman microprobe spectroscopy for the study of fluid inclusions. Geochim Cosmochim Acta 52:979–988

Peccerillo A, Frezzotti ML, De Astis G, Ventura G (2006) Modeling the magma plumbing system of Vulcano (Aeolian Islands, Italy) by integrated fluid-inclusion geobarometry, petrology, and geophysics. Geology 34:17-20

Pollard DD, Delaney PT, Duffield WA, Endo ET, Okamura AT (1983) Surface deformation in volcanic rift zones. Tectonophysics 94:541–584

Robertson AHF, Stillman CJ (1979) Submarine volcanic and associated sedimentary rocks of the Fuerteventura Basal Complex, Canary Islands. Geolog Mag 116:203–214

Roedder E (1965) Liquid CO_2 inclusions in olivine-bearing nodules and phenocrysts from basalts. Amer Miner 50:20–40

Roedder, E (1983). Geobarometry of ultramafic xenoliths from Loihi Seamount, Hawaii, on the basis of CO_2 inclusions in olivine. Earth Planet Sci Lett 66:369–379

Roedder E (1984) Fluid inclusions. Roedder, E. (1984) Fluid Inclusions. Reviews in Mineralogy Vol. 12. Mineral Soc Am, pp. 644

Rosso KM, Bodnar RJ (1995) Detection limits of CO_2 in fluid inclusions using microthermometry and laser Raman spectroscopy and the spectroscopic characterization of CO_2. Geochim Cosmochim Acta 59:3961–3975

Ryan MP (1988) Structure of Active Magmatic Systems' Kilauea Volcano, Hawaii. Journal of Geophys Res 93(B5): 4213–4248. http://doi.org/10.1029/JB093iB05p04213

Scandone R, Cashman KV, Malone SD (2007) Magma supply, magma ascent and the style of volcanic eruptions. Earth Planet Sci Lett 253:513–529

Schmincke HU (1982) Volcanic and chemical evolution of the Canary Islands. In: U VonRad et al. (eds) Geology of the northwest African continental margin. Springer Verlag, New York, pp. 273–306

Schmincke HU, Sumita M, (1998) Volcanic evolution of Gran Canaria reconstructed from apron sediments: synthesis of vicap project drilling. Proceedings of the Ocean Drilling Program, Sci Res 157:443–469

Schwarz S, Klügel A, Wohlgemuth-Ueberwasser C (2004) Melt extraction pathways and stagnation depths beneath the Madeira and Desertas rift zones (NE Atlantic) inferred from barometric studies. Contrib Mineral Petrol 147:228–240

Shaw HR (1980) The fracture mechanisms of magma transport from the mantle to the surface. Phys Magmat Processes 64:201-264

Sparks RSJ (2003) Forecasting volcanic eruptions. Earth Planet Sci Lett 210:1–15

Stroncik NA, Klügel A, Hansteen TH (2009) The magmatic plumbing system beneath El Hierro (Canary Islands): constraints from phenocrysts and naturally quenched basaltic glasses in submarine rocks. Contrib Mineral Petrol 157-165

826 Ulmer P (1986) NORM-Program for cation and oxygen mineral norms. Computer Library,
827 Institut für Mineralogie und Petrographie, ETH-Zentrum, Zürich, Switzerland.

828 van den Kerkhof AM (1988) The system CO_2–CH_4–N_2 in fluid inclusions: theoretical
829 modelling and geological applications. PhD Dissertation, Amsterdam Free University, pp.
830 206

831 Viti C, Frezzotti ML (2000) Re-equilibration of glass and CO_2 inclusions in xenolith olivine:
832 A TEM study. Amer Mineral 85:1390-1396

833 Viti C, Frezzotti ML (2001) Transmission electron microscopy applied to fluid inclusion
834 investigations. Lithos 55:125–138

835 Vityk MO, Bodnar R J (1998) Statistical microthermometry of synthetic fluid inclusions in
836 quartz during decompression re-equilibration. Contrib Mineral Petrol 132:149-162

837 Voog DB, Palomé SP, Hirn A, Charvis P, Gallart J, Rousset D, Perroud H (1999) Vertical
838 movements and material transport during hotspot activity: Seismic reflection profiling
839 offshore La Réunion. J Geophy Res 104:2855-2874

840 Wanamaker B.J, Evans B (1989) Mechanical re-equilibration of fluid inclusions in San Carlos
841 olivine by power-law creep. Contrib Mineral Petrol 102:102-111

842 Wang CH, Wright RB (1973) Effect of density on the Raman scattering of molecular fluids. I.
843 A detailed study of the scattering polarization, intensity, frequency shift, and spectral
844 shape in gaseous N2. J Chem Phys 59:1706-1712.

845 Wang X, Chou IM, Hu W, Burruss RC, Sun Q, Song Y (2011) Raman spectroscopic
846 measurements of CO_2 density: Experimental calibration with high-pressure optical cell
847 (HPOC) and fused silica capillary capsule (FSCC) with application to fluid inclusion
848 observations. Geochim Cosmochim Acta 75:4080–4093

849 Wells PR (1977) Pyroxene thermometry in simple and complex systems. Contrib Mineral
850 Petrol 62:129-139

851 Witt-Eickschen G, Seck HA (1991) Solubility of Ca and Al in orthopyroxene from spinel
852 peridotite: an improved version of an empirical geothermometer. Contrib Mineral Petrol
853 106:431-439

854 Wright RB, Wang CH (1973) Density effect on the Fermi resonance in gaseous CO_2 Raman
855 scattering. J Chem Phys 58: 2893–2895

856 Wulff-Pedersen E, Neumann ER, Jensen BB (1996) The upper mantle under La Palma,
857 Canary Islands: formation of Si−K−Na-rich melt and its importance as a metasomatic
858 agent. Contrib Mineral Petrol 125: 113–139

859 Zanon V, Frezzotti ML, Peccerillo A (2003). Magmatic feeding system and crustal magma
860 accumulation beneath Vulcano Island (Italy): Evidence from CO_2 fluid inclusions in quartz
861 xenoliths. J Geophy Res 108:2298 http://doi.org/10.1029/2002JB002140

862 Zanon V, Frezzotti ML (2013) Magma storage and ascent conditions beneath Pico and Faial
863 islands (Azores archipelago): A study on fluid inclusions. Geochem Geophys Geosyst
864 14:3494–3514

865 Zaczek K, Troll VR, Cachao M, Ferreira F, Deegan FM, Carracedo JC, Meade FC, Burchardt
866 S (2015) Nannofossils in 2011 El Hierro eruptive products reinstate plume model for
867 Canary Islands. Sci Rep 5, 7945. http://dx.doi.org/10.1038/srep07945.

868

869

870 **Figure Captions**

871

872

873 Fig. 1 - **a** Geographical setting of the Canary Islands showing the age of the volcanism and the
874 stages of the volcanic island growth (Shield stage, Post-erosional stage, Post-shield gap),
875 (modified from Carracedo 1999, Acosta et al. 2005). The yellow lines define the main
876 structures of Atlantic and African tectonic units; **b** Geographical setting of El Hierro Island
877 reporting xenolith sampling locality in El Julan cliff Valley (red star).

878 Fig. 2 - **a** ultramafic xenoliths in the basaltic lava outcrop of El Julan cliff Valley; **b – h**
879 microphotographs of studied peridotites. **b** Deformed olivine porphyroclasts (Ol I) in
880 spinel harzburgite (XML9, crossed polarizers); **c** Orthopyroxene porphyroclasts (Opx I)
881 with exsolution lamellae of clinopyroxene (Cpx) in spinel lherzolite (XML8, crossed
882 polarizers) **d** Exsolved Opx I with rims free of exsolution lamellae in spinel harzburgite
883 (XML7, parallel polarizers); **e** Opx I without exsolution lamellae in spinel harzburgite
884 (XML4, parallel polarizers); **f** Olivine neoblasts (Ol II) forming triple junctions in spinel
885 harzburgite XML7, crossed polarizers; **g** Neoblast assemblage of Ol II + Opx II + Cpx +
886 Sp in spinel lherzolite (XML3, crossed polarizers); **h** Ol II forming narrow alignments
887 cutting Ol I in spinel dunite (broken yellow lines) (XML1, crossed polarizers).

888 Fig. 3 - Microphotographs of early Type I fluid inclusions in low temperature (LT)
889 peridotites; **a** Intragranular trail of Type I fluid inclusions in Ol I (harzburgite XML7,
890 parallel polarizers); **b** carbonate (high birefringency) in fluid inclusions and microveins
891 (red arrows) in Ol I (harzburgite XML7, crossed polarizers); **c** cluster of Type I fluid

892 inclusions in Opx I (harzburgite XML7, parallel polarizers); **d** multiphase Type I fluid
893 inclusion containing several daughter minerals and showing evidence for partial
894 decrepitation (red arrows in Ol I (harzburgite XML7 parallel polarizers).

895 Fig. 4 - Raman characterization of daughter mineral phases in a single Type I fluid inclusion.
896 **a** Photomicrograph showing distribution of daughter mineral phases in inclusion based on
897 Raman mapping: anhydrite (Anh), dolomite (Dol), sulfohalite (Shl), $MgSO_4+H_2O$, apatite
898 (Ap), spinel (Sp), and CO_2+N_2 fluid; **b-f** Raman spectra of daughter mineral phases; **b**
899 apatite; **c** anhydrite; **d** water in $MgSO_4*nH_2O$; **e** anhydrite, sulfohalite, and dolomite; **f**
900 spinel and anhydrite. Numbers in spectra report Raman modes of identified phases in cm^{-1}.
901 Asterisks indicate host mineral vibrations.

902 Fig. 5 - Microphotographs of Late Type II fluid inclusions in LT and HT peridotites. **a**
903 intragranular trails (red arrows) in orthopyroxene porphyroclast and clinopyroxene; **b**
904 decrepitated fluid inclusions in an olivine porphyroclast; **c** isolated cluster of fluid
905 inclusions (red arrows); **d** fluid inclusions distributed parallel to exsolution lamellae (red
906 arrows) in an orthopyroxene porphyroclast.

907 Fig. 6 - Histogram of CO_2 melting temperatures (Tm) for Type II fluid inclusions, and final
908 CO_2 melting temperatures (Tm) for Type I fluid inclusions. n = number of measurements.

909 Fig. 7 - **a** Composition (X_{N2}) and molar volume (cm^3/mole) of Type I CO_2 - N_2 fluid
910 inclusions from a single cluster. black numbers = X_{N2}; yellow numbers = molar volume
911 (cm^3/mole) =; **b** and **c** Raman spectra of CO_2 and N_2; (Δ) = distance of the Fermi doublet
912 in CO_2 Raman spectra.

913 Fig. 8 – Isochore (cm^3/mole) distribution in the T-X diagram for the CO_2 – N_2 system
914 (modified from van den Kerkhof 1988 and Klemd et al. 1992). Measured phase transition
915 sequences for S4 and H3 Type I CO_2 – N_2 fluid inclusions of known composition allow

916 determining molar volumes (green dots). S = solid; L = liquid; V = vapor; Th =
917 homogenization temperature.

918 Fig. 9 - Histogram of CO_2 homogenization temperatures (ThL) for Type II fluid inclusions.
919 Ol = olivine; Opx = orthopyroxene; Cpx = clinopyroxene; n. = number of measurements.

920 Fig. 10 - Histograms of CO_2 homogenization temperatures (ThL) for Type II fluid inclusions
921 in LT (a) and HT (b) peridotites. Abbreviations as in Fig. 9.

922 Fig. 11 - Histograms of CO_2 homogenization temperatures (ThL) for Type II fluid inclusions
923 showing data distribution in the different minerals. Abbreviations as in Fig. 9.

924 Fig. 12 - Distribution of CO_2 density values for Type II fluid inclusions in LT (a) and HT (b)
925 peridotites. See text, for discussion. Abbreviations as in Fig. 9.

926 Fig. 13 - CO_2 isochore (g/cm^3) distribution in the P-T diagram for Type I and Type II fluid
927 inclusions in LT and HT peridotites. Yellow arrows indicate the ascent path of LT and HT
928 peridotites at the considered temperatures. The pink star indicates pressure conditions
929 recorded by Type I fluid inclusions in LT peridotites. Green and blue stars indicate
930 pressures of deep trapping of Type II CO_2 fluids in LT and HT peridotites, respectively.
931 Red stars indicate pressures of shallow trapping of Type II CO_2 fluids in LT and HT
932 peridotites, respectively.

933 Fig. 14 - Proposed model for the magma plumbing system of El Hierro volcano at 40-30 ka. A
934 deep-seated reservoir is identified in the shallow lithospheric mantle at depths from
935 approximately 37 to 22 km. A short-lived shallower reservoir located in the lower oceanic
936 crust at 12-10 km. See text for discussion. The black star = source of mantle xenoliths.

Dear Eduardo

First of all, I apologize for it has taken so long to get your manuscript reviewed. This was mainly

because one reviewer was away for a long time.

Nevertheless, we now received 3 reviews that are overall positive, and I think that the paper needs moderate to major revision. The reviewers identified several problems and all commented on poor English. For example, one reviewer is concerned that "Manuscript is in need of careful final edits with attention to the small details of grammar, English, and bits of missing text". As to the manuscript topic, data and conclusions, I agree with Thor Hansteen, who found your results on different daughter phases ("carbonates + sulphates, ± chlorides ± phosphates ± opaque minerals") are of particular interest, but also considered the implications for the magma ascent from the inclusions' CO2 density in your paper to have been reported before and thus being "standard". This makes me wonder whether you are willing to make your publication more exciting by discussing compositions of the carbonate-sulfate melts in the lithospheric mantle, their origin (big question mark) and contribution to peridotite-derived silicate melts. I personally welcome this new information to be presented in Bulletin of Volcanology, if your submission to Chemical Geology (Villa et al., Halogens in the lithospheric mantle beneath El Hierro) is unsuccessful.

I also agree with Frances Deegan that you make references to other papers without actually discussing other people models in the context of your data. In a covering letter appended to your revised manuscript, you must explain how you have addressed the comments made by all reviewers. If you disagree with any of the comments please clearly explain why.

My recommendations and the reviewers' comments can be found at the end of this email.

Reviewer #1: Review of the manuscript "Lithospheric magma dynamics beneath El Hierro, Canary Islands:

a fluid inclusion study" by E. Oglialor1, M.L. Frezzotti, S. Ferrando, C. Tiraboschi, C. Principe, G. Groppelli,

and I.M. Villa

General comments:

This is a potentially interesting paper with a comprehensive original data set on fluid inclusions in mantle xenoliths from El Hierro Island. The data are utilized to tell an interesting history of mantle fluid origin and xenolith ascent. The new and innovative feature is the detailed description of carbonate and sulphate phases occurring in the early fluid inclusions, indicating a complex chemistry of the originally trapped mantle fluids. However, the fluid inclusion data set is used to describe the magma ascent history of the host magmas and thus make inferences about the magma plumbing system of El Hierro, and the conclusions reached are rather similar to the conclusions forwarded by other authors for other eruptions of El Hierro. Thus the conclusions drawn in the paper are valid and good, but except for the refined suggestions about the nature of early fluid inclusions in the peridotites, they are fairly standard. The manuscript in its present form contains several errors and inaccuracies, and the English should be checked before resubmission. Thus a major (thorough) revision is recommended. The most important points are listed below.

Response – We have better detailed the rationale of our study in the introduction. Present study reveals the depths of lithospheric sub-Moho magma storage regions at El Hierro. Further, studied rocks are the deepest example of peridotites beneath the Island. In addition, complex metasomatic fluids are reported.

Most existing information of the deep internal structure of this volcano are coming from the 2011-2012 eruption's earthquake hypocenters. Our data collectively allow for the first time to propose a model for

the deep magma dynamics beneath the Island. No previous studies on mantle rocks have revealed in a similar detail the deep magma dynamics, although several petrological studies have been performed in mantle xenoliths from El Hierro.

Selected specific comments:

The Abstract could be more to the point in its opening sentences. Please also indicate that you use xenoliths to reconstruct the stagnation depths in the magma plumbing system of the host lavas. Further, there is no mention of model temperatures used in the barometry calculations for the multi-stage ascent model.

Response – The abstract has been rewritten following your suggestions

Methods chapter: There is potential problem with the unusually high pressures you derive from the one early CO2-N2 fluid inclusion with a very high density of 1.191 g/cm3. This inclusion is used to address the depth of xenolith origin. Using the equation of state of Holloway (1977), you obtain a pressure of about 1.8 GPa. A density of 1.191 g/cm3 for pure CO2 would, however, result in a pressure of 1126 MPa at 950 °C using the EOS of Sterner and Pitzer 1994. Please discuss the validity of such presented high pressures.

Response – We would respectfully disagree with you here. The relations between P, T, V and X in supercritical fluids of geological interest are expressed by the equations of state. These also consider the attractive and repulsive forces and volumes of molecules (e.g., a and b parameters of van der Waals equation). Thus, equations of state for fluid mixtures should consider the application of mixing rules (i.e., Redlich and Kwong 1949). As a consequence, an equation for a CO2-N2 mixture having the same molar volume of a pure CO2 fluid will not calculate the same P or T values.

Discussion chapter: Altogether, pressures are calculated for both early and late fluid inclusions in the xenoliths. Although magma stagnation levels for the host magmas are evaluated from the data, model temperatures shown in the P,T-diagram are set to 1000 °C and 950 °C, respectively. Taken the time the xenoliths were in magma contact, why do you not use estimated magma temperatures? Do the late fluid inclusion trails reach xenolith surfaces? Do some of the late FI coexist with melt inclusions?

Response - We appreciate this comment. Indeed we needed to be more clear in terms of selection of model temperatures. We added these clarifications in the fluid inclusion sections. We did not use the magma temperatures since the densities of fluid inclusions reflect differences in temperatures of LT and HT peridotites. We have, however, considered as model temperatures the higher values of each interval.

Abstract

Line 25: " .. late pure CO2 fluid inclusions trapped during the ascent into the host magma." What is the evidence for trapping during ascent? Or do you infer this from the pressure data?

Response - We infer this from pressure data. Text has been modified.

Introduction

Line 82-86: You state that the magmas "rest" (stagnate) on their way to the surface, but then write: "Results indicate, for the first time, that the magma ascent in the lithospheric mantle occurs as a continuous migration through a plexus of vertically stacked interconnected magma pockets..". Please explain.

Response – We agree that the sentence was contradictory. We have eliminated this part.

Geological setting and volcanic history

Line 88-92: Please mention here the various mantle plume hypotheses for the Canary Islands.

Response – We have added the mantle plume hypothesis and other concurrent hypotheses.

Methods

Line 174 -175: Please check the pressure calculations for the mixed CO2-N2 fluid inclusions (see comment above)

Response – see comment above.

Fluid inclusion study

Line 303-309: Do the Late Type II fluid inclusions trails partly extend to xenolith surfaces? Are some trails melt-present (coexistence of melt and fluid inclusions)?

Response. Trails are not extending to xenoliths surfaces and they do not contain basaltic melt/glass. This is quite commonly seen in deep (mantle depth) fluids trapped in xenoliths. We have better detailed this observation in the petrography of peridotites.

Discussion

Line 381: You state: "Fluid inclusions in mantle xenoliths represent either metasomatic fluids in the lithosphere, unrelated to xenoliths transport to the surface, or fluids degassed by the ascending magmas during xenolith ejection at the surface.."

This is unclear: The magmatic fluids may relate to the host magma, or alternatively to an earlier batch of magma at the xenolith source depth. Please reformulate this sentence.

Response – Reformulated.

Line 386+: You state: "The densities of metasomatic and magmatic fluids are generally different, since trapping occur at different pressure conditions." This is inaccurate: There are also large temperature variations at a given depth, according to the presence or absence of magma. Please reconsider this sentence.

Response - We agree. We have rewritten the sentence "The densities of metasomatic and magmatic fluids are generally different, since trapping occur at different pressure and temperature conditions."

Line 405-406: Should read: "…which corresponds to magma stagnation episodes at defined depths.."

Response - OK

Line 464: Please delete the sentence "Fluxes of CO2 probably originated by magma degassing episodes."

Response - OK

Line 497-498: You state. "The densest among Type I CO2-N2 mantle metasomatic fluids suggests 60 km as the minimum equilibration depth in the lithosphere for LT peridotites (grey star in Fig. 14; P = 1.80 ± 0.02 GPa)." Please reconsider this sentence based on the comments above.

Response – Data are derived from geothermobarometry of CO2-N2 fluids. We should be aware that deep mantle fluids can be more complex than pure CO2. This is evident whenever fluid inclusion studies

include Raman analyses. Raman in fact represent the most powerful analytical technique to detect small amounts of gaseous species in CO2-rich fluids. Most previous studies of fluid inclusions in mantle xenoliths from El Hierro did not detect N2 in CO2-rich fluid inclusions. These studies, however, did not include Raman among the analytical techniques.

Line 541: You state "One main result from present study is that it resolves the geometries of the magma storage system in the lithospheric mantle." I regret to say that this is strictly not correct. The methods used only indicate pressure conditions based on suggested model temperatures, but give NO evidence of the remaining magma plumbing geometry. Please reformulate this sentence.

Response - We agree. We have deleted all text parts dealing with "geometry" of the magma storage system.

Conclusions

Line 561-562: You state: "Our observations are consistent with a deep magma source beneath El Hierro volcano, in agreement with the previous models for last eruption in 2011-2012". This is not to the point as your paper is about magma plumbing systems and ascent, not about magma sources.

Response - We agree. We have eliminated the sentence.

Line 563-565: You state: "Finally, present paper demonstrates the potentiality to study the geometries of deep magma reservoirs by fluid inclusion studies in peridotites, when combined with detailed petrological investigations of rocks". This is too general and thus unfocussed. Please reformulate.

Response - We agree. We have eliminated the sentence.

Technical comments:

Please do not start mineral names with a capital letter (as in the captions to Figures 4 and 5)

Response. We have fixed it.

Best wishes

Thor Hansteen

Reviewer #2: Review of "Lithospheric mantle dynamics beneath El Hierro, Canary Islands: a fluid inclusion study" by Eduardo Oglialoro et al., submitted to Bulletin of Volcanology.

The manuscript by Ogliarloro et al. presents new fluid inclusion data on ultramafic xenoliths from El Hierro, Canary Islands, in order to contribute to a clearer picture of the magma plumbing system beneath the island. The authors' new results show that El Hierro magmas originate from vertically stacked reservoirs in the lithospheric mantle, which is consistent with the results of previous thermobarometry studies (e.g. Stroncik et al., 2009; Longpre et al., 2014). Overall, I think that this work will make a worthy contribution to our understanding of magma storage and ascent at ocean island volcanoes. However, I have some issues with how the paper is written and I think that it needs an overhaul of the writing in order to improve grammar and syntax and hence accessibility (the figures are of good quality). An improved writing style will require a little more effort but will help the results to be assimilated more easily by the community. I also think that the literature needs to be integrated into the discussion more fully. At the moment, many papers

are cited but not really discussed and compared to the new data. Finally, I think that the authors can make more of an effort with the thermobarometry aspect in terms of updating their own calculations, comparing them to the literature data, and linking them with their new fluid inclusion data. I feel that this would help to strengthen the paper's conclusions.

Some points are expanded on below:

1. The existing literature should be better integrated and discussed in this paper. For example, the introduction and geological background of the manuscript lack a balanced overview of the recent literature on the geology of El Hierro and, in particular, the 2011-2012 submarine eruption. You have mentioned some of the efforts that have been employed to characterize magma dynamics at El Hierro (lines 61 – 64), but you have overlooked a body of work concerning the "floating stones" that were erupted in 2011-2012 and their implications for magma dynamics and magma plumbing at El Hierro (e.g. Troll et al., 2012 in Solid Earth; Zaczek et al., 2015 in Scientific Reports; Berg et al., 2016 in Bulletin of Volcanology). Where you mention "independent analytical approaches" that have been employed to study the plumbing system at El Hierro on line 65, you should also mention "xenolith studies" and cite some relevant literature. The floating stones were highly informative regarding our understanding of magma transport and crustal interaction at El Hierro. I realise that the shallow plumbing system is not the focus of your study, but this work should be at least mentioned in your introduction in order to put your study into context. Furthermore, a review of the 2011-2012 submarine eruption was published in Earth Science Reviews in 2015 by Carracedo et al. (http://dx.doi.org/10.1016/j.earscirev.2015.06.007). This paper offers a detailed review of the events leading up to, and during, the 2011-2012 eruption and includes discussion of the plumbing system at El Hierro making it highly relevant to your study. Lastly, Longpre et al. have recently published volatile data obtained on samples from the 2011-2012 in Earth and Planetary Science Letters, which may be very useful for discussion of your data (Longpre et al., 2017).

   Response - **We agree. We were missing some relevant literature. In the present version of the manuscript we have added and discussed all literature indicated by you, including Carracedo et al., 2015, Longprè et al., 2017, Zaczec et al., 2015. In particular, data from Longprè suggesting very deep degassing of CO2 El Hierro mafic magmas well agree with our finding of CO2 fluids at pressure of 1 GPa.**

2. I think it would be worthwhile to look into the literature regarding other Canary Islands too. For example, Barker et al. 2015 (DOI 10.1007/s00410-015-1207-7) use mineral thermobarometry and mineral-melt thermobarometry to define the sub-volcanic magma plumbing system for La Palma, Canary Islands. These authors found evidence for magma storage at sub-Moho depths of up to 50km and they discuss various magmatic processes during magma storage such as recycling of pre-existing ocean island plutonic complexes. This paper is thus highly relevant to your work on the deep plumbing system at El Hierro and ought to be discussed.

   Response - **We are grateful for this comment. We have discussed data from La Palma by Barker and coauthors, which, as you suggersted, share several similarities with present results.**

3. Many of the literature citations in the text do not match the reference list or cannot be found there. These occurrences are too numerous to list here. Please check all literature citations very carefully. Also avoid a) and b) where not necessary e.g. Frezzotti and Peccerillo (2004) does not need to be written as Frezzotti and Peccerillo (2004a).

Response - We have corrected these issues.

4. Regarding thermobarometry, have you tried using your pyroxene data to calculate crystallization temperature and pressure? I suggest using several models and also incorporating more recent approaches (it seems to me that you have used fairly old models) and comparing the outcomes. Do you get consistent values? Are these values consistent with the results of your fluid inclusion study? Please see Geiger et al. 2016 in Scientific Reports (DOI 10.1038/srep33629) and references therein for some examples of recent model developments in thermobarometry, with particular application to alkali systems. It would make your paper a much more useful contribution stronger if you follow up on the thermobarometry more thoroughly and link it to your fluid inclusion data. If it turns out that other thermobarometric models are not suitable for your samples, then explain why.

Response – We respectfully disagree. We have not used fairly old geothermobarometers. We have applied geothermobarometry based on mineral equilibria in mantle rocks. Melt-mineral geothermobarometry in host basaltic rocks is not part of present study.

5. The manuscript text needs substantial polishing before it is publication-ready and I suggest that you ask a colleague to carefully proof-read your manuscript text for fluency before resubmission. I also think that you need to make very clear the reasons for undertaking this study. As noted above, the plumbing system beneath El Hierro has been extensively studied already. What new insights can your method of choice bring?

Response – We agree. We have carefully rewritten the text. The new insights of our methods are on the deep internal structure of the volcano. When rewriting the text, we have clarified this issue.

If the authors can address the points above then I think that this paper would make a welcome contribution to our understanding of the plumbing system at El Hierro, but it first needs to undergo major revision. I would be happy to re-read a revised version.

With best regards,

Frances Deegan, Uppsala University, April 2017

Reviewer #3: Hello

I think this paper is pretty good. It really needs a careful final edit, however, looking for mistakes of grammar and English, as well as putting in a few missing words here and there.

Below are specific issues I found that I think need to be changed or thought about, and most involved making the paper read more clearly, and limiting overly dramatic and overreaching language that is not needed in this paper. Below are some specific examples of edits to consider, but they are not all the small issues. Please comb over carefully.

Cheers.

Abstract

18-19

This opening sentence needs rewriting. Fluid inclusion studies are one example of petrologic investigations, not a unique field themselves, and volcanological data (as I think of it) do not actually help define or constrain any of the parameters of depth of storage, or pathways through plumbing. Petrology does.

Response - We agree. We have changed the text following your suggestions.

31-34

Here again...the term (or phrase) 'eruption dynamics' is not appropriate here. This is not what this study is showing. There is nothing about 'eruption dynamics' at all in these data. It would more appropriate to refer to "magma dynamics".

Response - We agree. We have changed the text following your suggestions.

These FI data are providing data to infer what conditions the magma (or more correctly, the xenoliths) had experienced. The data are from a 'time' that is well before the 'eruption' and may not have any bearing on the eruption dynamics at all. This is important. The study is about magma pathways and storage levels during ascent from the mantle and through the crust, not about the dynamics of an eruption.

Response - We agree. We have changed the text following your suggestions. Present study further allows presenting a model for magma pathways that is very similar to magma dynamics during the 2011-2012 eruption. In additions, xenoliths are hosted in erupted lavas.

34-37

Here it is finally right. This is about magma dynamics, and whether magma dynamics inferred from 50ka FIs show the same/similar behavior as the recent erupted magma.

Response – We agree. See comment above.

Introduction

39-40

Cut 'prerequisite'…redundant with essential…"Modelling…is essential to evaluate the monitoring strategies…"

Response - We agree. We have changed the text following your suggestions.

41

Cut hence…"pressure and depth"…

"Rest"…better to say "storage and/or accumulation".

Response - We agree. We have changed the text following your suggestions.

55-58

Do you mean these studies have already been carried out? Sounds like they have not been… 'Proposed' probably meant to say 'performed'.

Response - We agree. We have changed the text following your suggestions.

64

The proposed model…

76

(2004), we have performed…

80

…magma ascent and periodic storage…

81

Cut out "…for the first time…" . May or may not be true and hard to verify.

81-84

Response - We agree. We have changed the text following your suggestions for all points listed above.

This last sentence of the intro seems to contradict the earlier setup, and perhaps the data to follow. Either the magma pauses or is stored long enough for fluid to invade and be trapped by host crystals, or not. To say that magma ascent is a "continuous" migration is likely an overreach at this point since discreet levels have been identified using geophys and are likely regions of pooling, or storage areas…direct contradiction to the idea that magma is in a continuous migration!

Response - We agree. We have changed the text following your suggestions.

Geo Setting

Generally OK.

Methods

Fairly clearly written.

Comp and P-T…

192-201

Rewrite this paragraph to be more succinct. Is the flow the same as Carracedo's 2001 lava, or different? There should be no confusion, and no need to deduce if it is the same. Did you walk from Carrecedo's site to yours and know it's the same? It is or it isn't. It probably doesn't really matter, and this paragraph is overcomplicating the issue. So, it's about 50ka or a bit younger based on Carrecedo's ages in the area on similar flows.

Response - We have simplified the text following your suggestions.

203-204

"The contours of rocks are sharp"…what does this mean, angular? Clean? Do they have any basaltic coating? You say they have limited host lava infiltrations? Please clarify with a picture or better description. Since you have seen some infiltration, this implies the xenos are warm to hot. How might this affect the preservation of the FI, and their chemistries? Do the xenos show any melt channels forming?

Response - Angular. Xenoliths with evidence for lava infiltrations were not selected for mineral geothermobarometry and fluid inclusion studies. We have changed the text.

Petrography

Written OK, but I have to say that after reading the petrologic description, I have questions about faithful, robust records preserved. The description suggests significant recrystallization and perhaps areas of remelting. Hmmm. Is this a problem?

Response - Xenoliths show protogranular textures with minor of solid state recrystallization (< of 30 %). This is indicative of moderate recristallization at mantle depths. In higher temperature xenoliths (900°C), evidence for variable sub-solidus heating is revealed by the presence of neoblasts and non clear opx porphyroclasts. Microstructural evidence for incipient melting of xenoliths in ascending lavas is absent in studied peridotites. Cpx and or spinel do not show evidence of incipient melting (e.g., spongy rims).

Mineral Chemistry

Noting that Ca increases in some neoblastic Ol is important. What is this saying about CPX? Is there a history of heating these xenos and melting of CPX? Does it matter, or not?

Response – Evidence for melting of Cpx is absent (i.e no spongy texture). In addition, Cpx is in textural equilibrium with the other mineral phases. Local heating is observed to about 1100°c degrees limited to Opx neoblasts. The Ca content of Cpx is considered by the two-pyroxene thermometer, and by the solubility of Ca and Al in orthopyroxene in equilibrium with olivine, clinopyroxene and spinel thermometer.

Geothermobarometry

I am concerned about these equilibrium temperature estimates…ALL seems too cool to be correct for these rock compositions. Shouldn't these temps be more >1100-1200C if they formed in the mantle? I suspect these are re-equilibration temperatures from being in the basalt. This is not clearly stated here (I see it later.), and the reader should be assured the authors know that the minerals used for FI have been survived r-e without leaking or cracking FI.

Response – We respectfully disagree. Calculated temperatures for peridotites are not too cool at the considered depths in the mantle. They correspond to geotherms with heat flow > 70 mW/m2 at 60 - 65 km depth. We imagine that "too cool" is referred an oceanic mantle geotherm.

Fluid Inclusion Study

This most important section is well-written and descriptive.

Discussion and conclusion

I liked these sections. Well written and described. My only criticism is the over statement that this study somehow reveals "geometry" of the magma plumbing system. It really does not. These data only tell that some components of the magma were sourced deep, then stored at mid and shallow crustal levels. Beyond the presumption that there is a vertical movement of material beneath El Hierro (as generally believed for any volcano), no other geometric info can be gleaned. Dial back these statements to be more considerate of this fact. FI data verify what the geophys already sees.

Response – We agree with you. We have eliminated the word: geometry.

Good overall.

Fig.1.JPEG

Click here to download Figure Fig.1.jpg

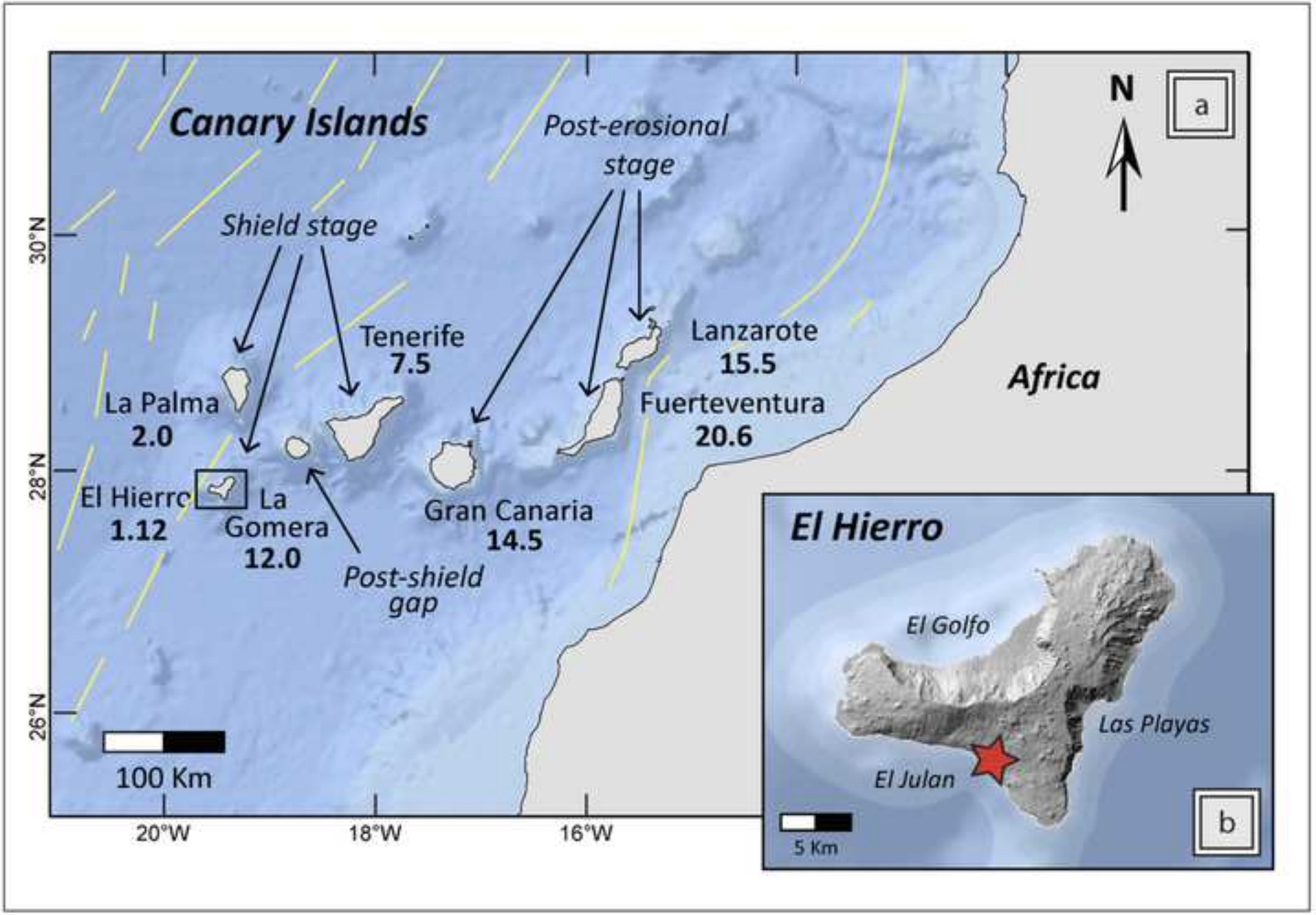

Fig.2.JPEG

Click here to download Figure Fig.2.jpg

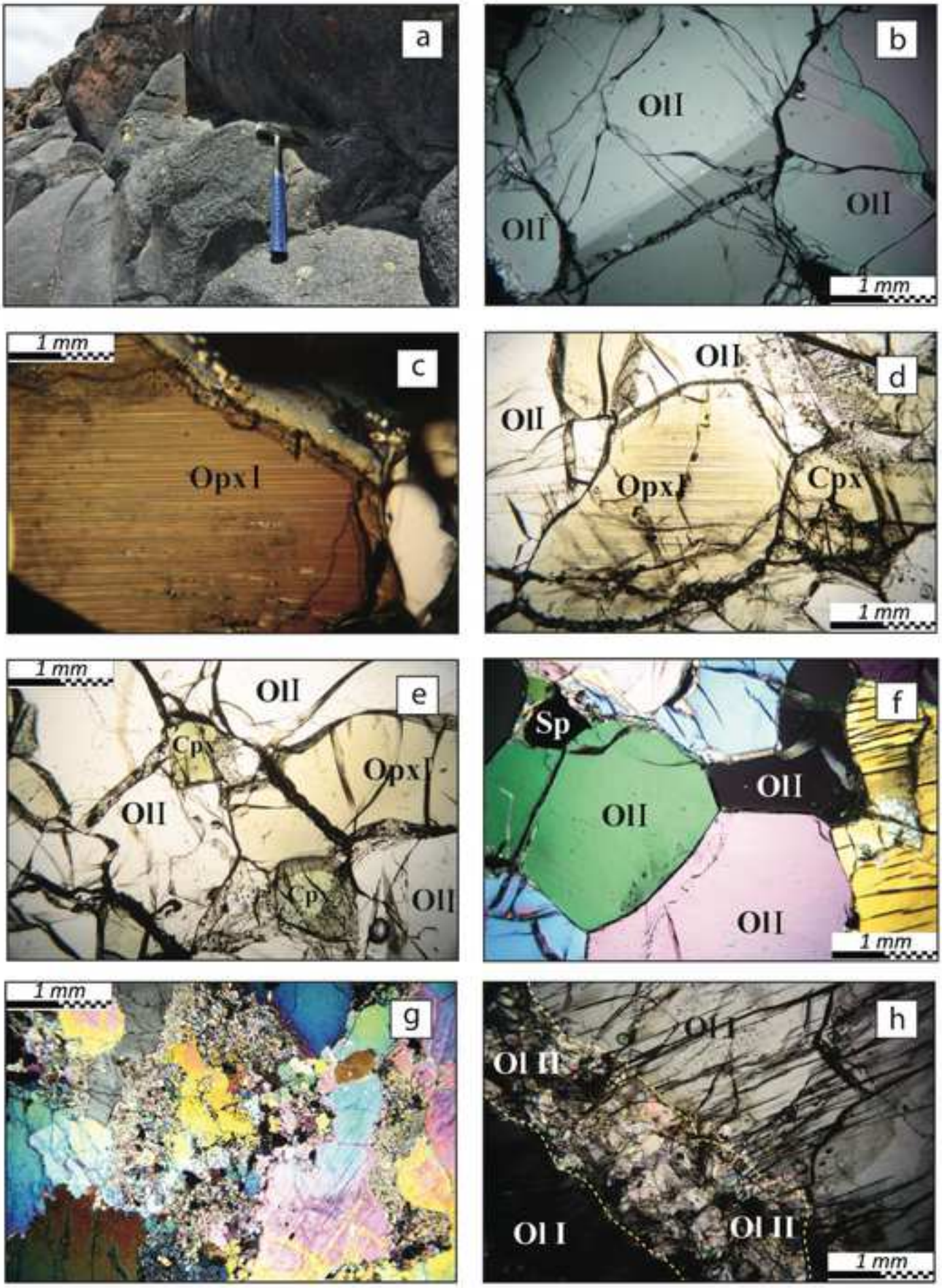

Fig.3.PNG

Click here to download Figure Fig.3.png

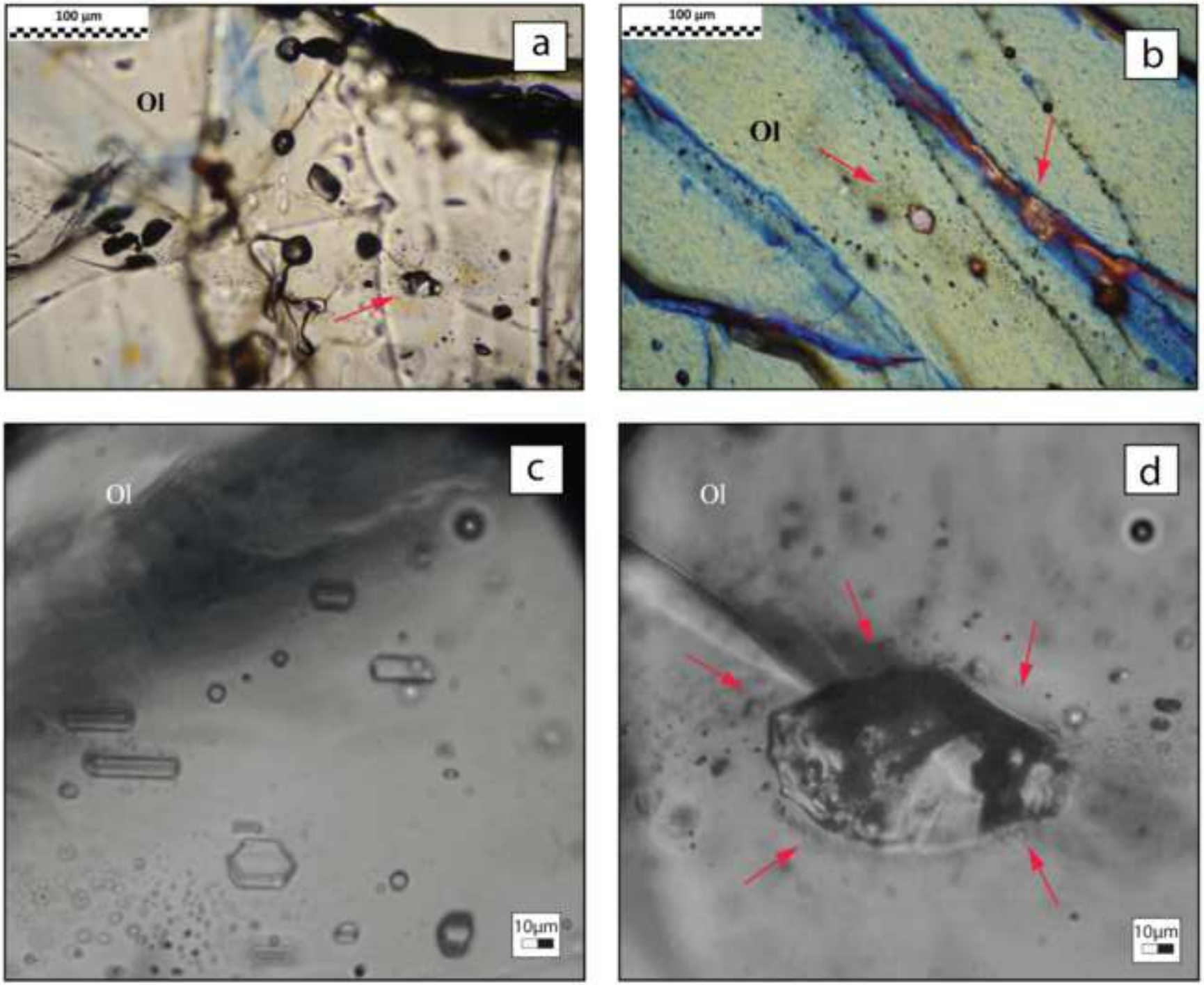

Fig.4.TIFF

Click here to download Figure Fig.4.tif

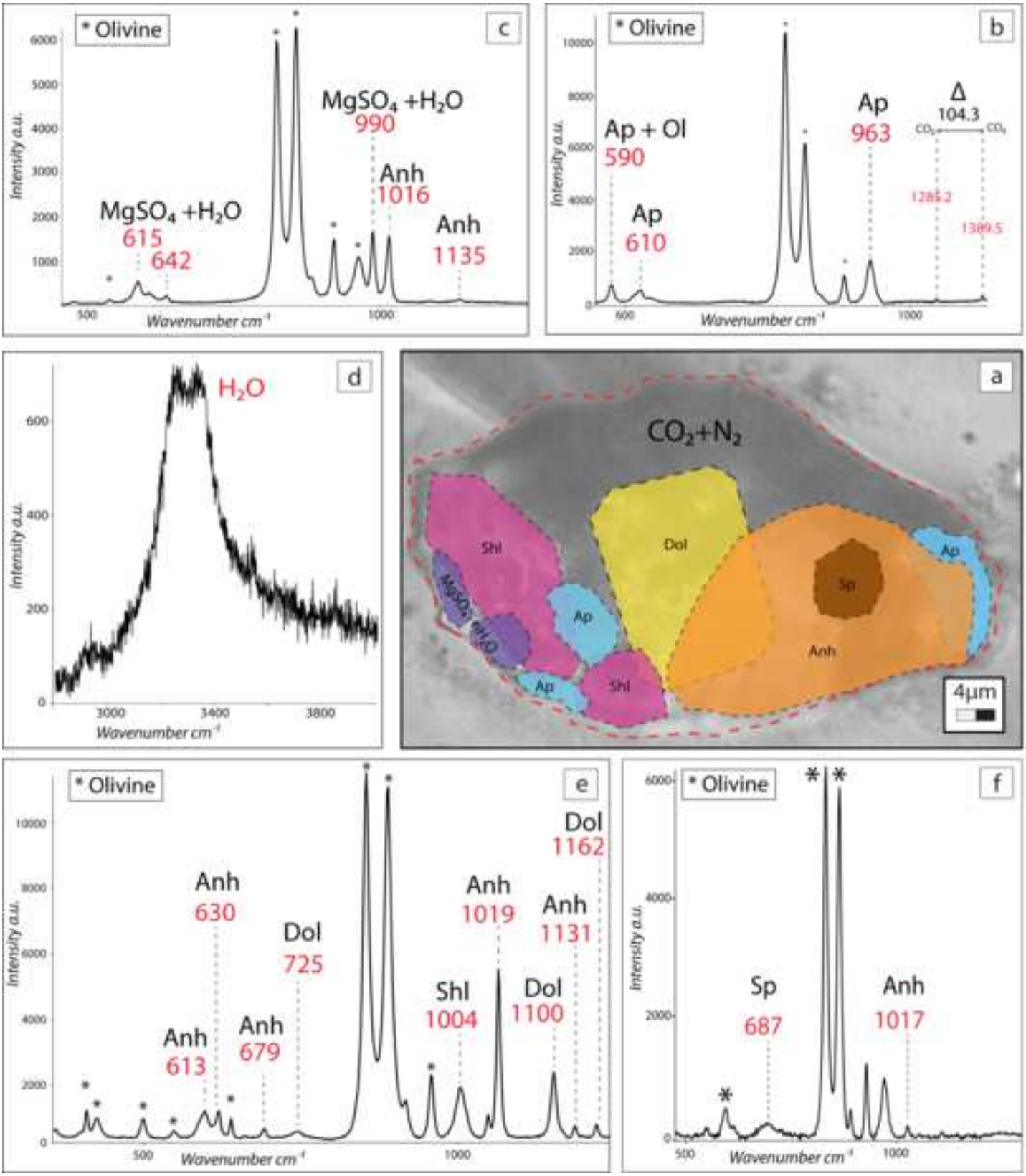

Fig.5.JPEG

Click here to download Figure Fig.5.jpg

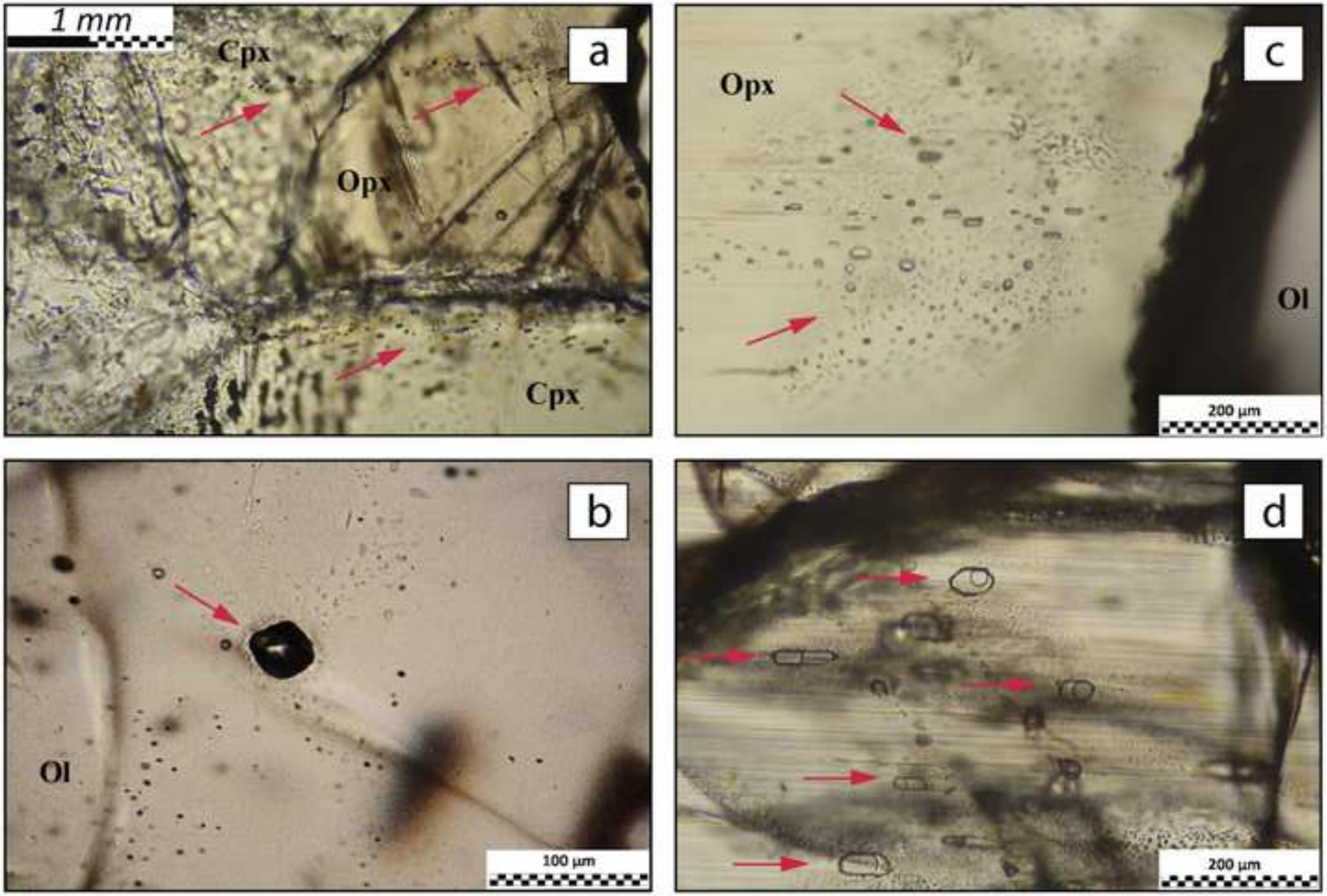

Fig.6.JPEG

Click here to download Figure Fig.6.jpg

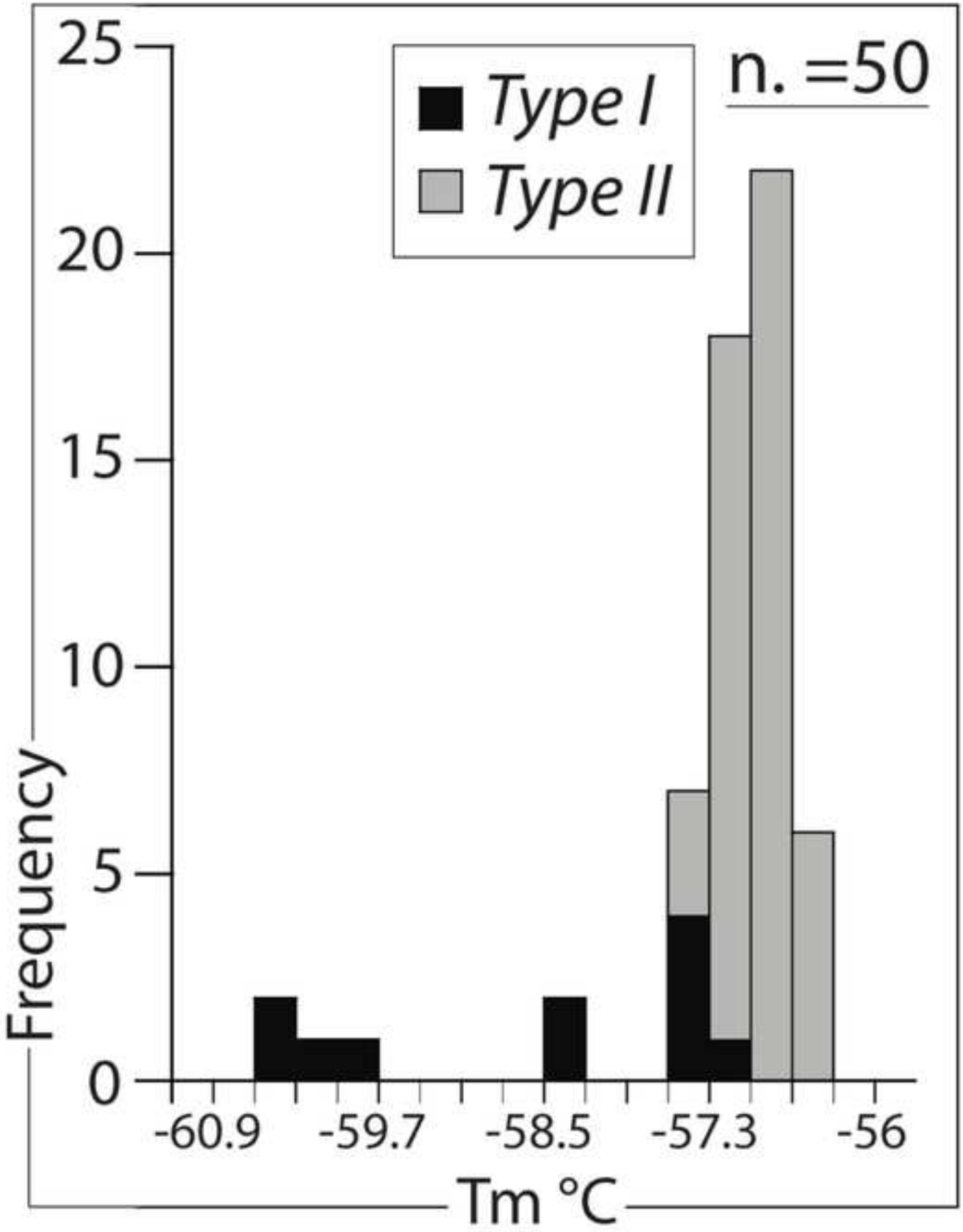

Fig. 7 PDF

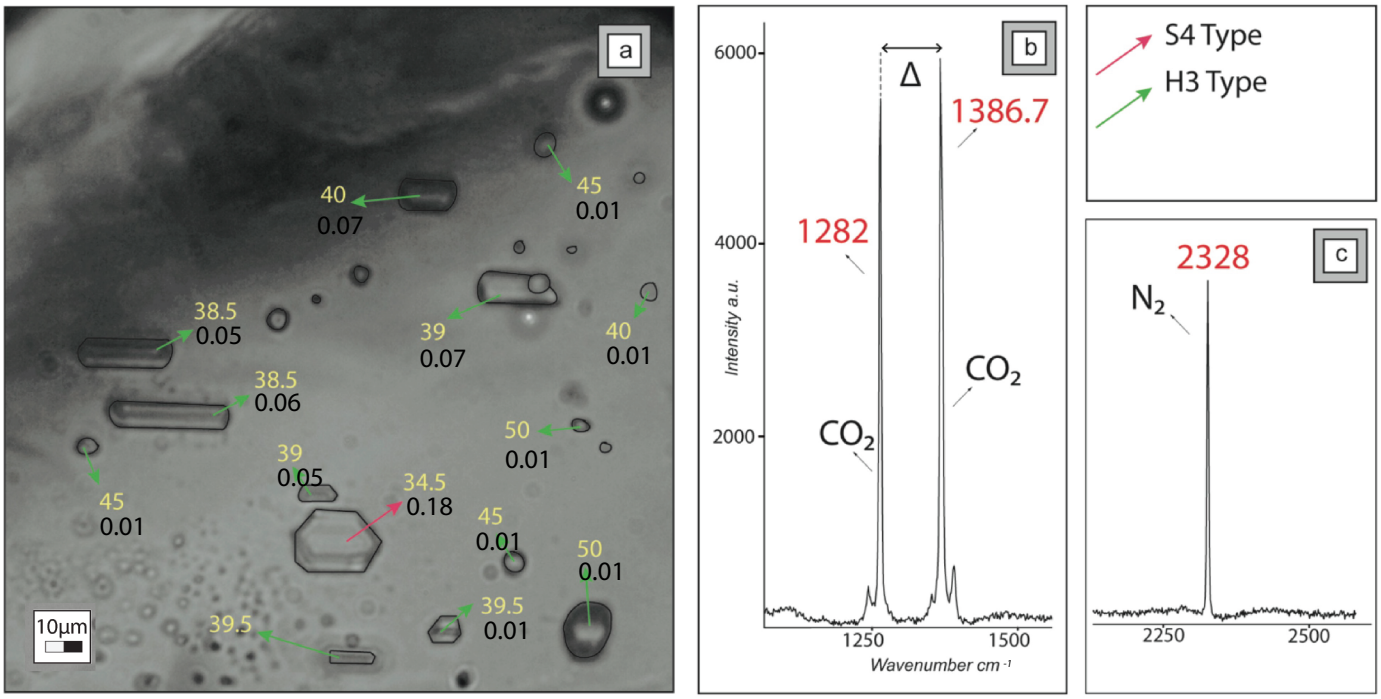
a
40
0.07
45
0.01
38.5
0.05
39
0.07
40
0.01
38.5
0.06
50
0.01
39
0.05
34.5
0.18
45
0.01
45
0.01
50
0.01
39.5
39.5
0.01
10µm
b
6000
4000
2000
Intensity a.u.
Δ
1386.7
1282
CO2
CO2
1250
1500
Wavenumber cm -1
S4 Type
H3 Type
c
2328
N2
2250
2500

Fig.8.JPEG

Click here to download Figure Fig.8.jpg

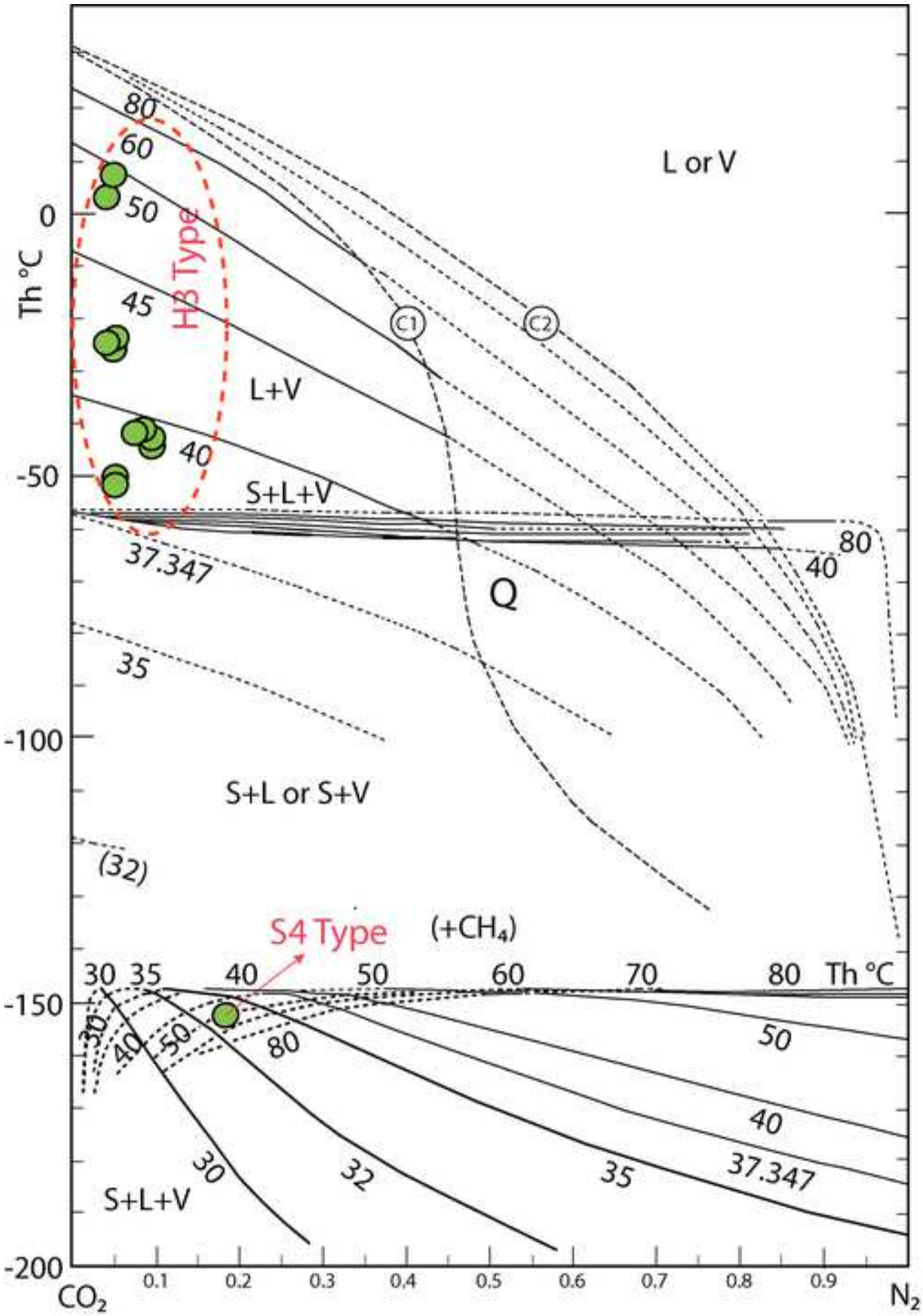

Fig.9.JPEG

Click here to download Figure Fig.9.jpg

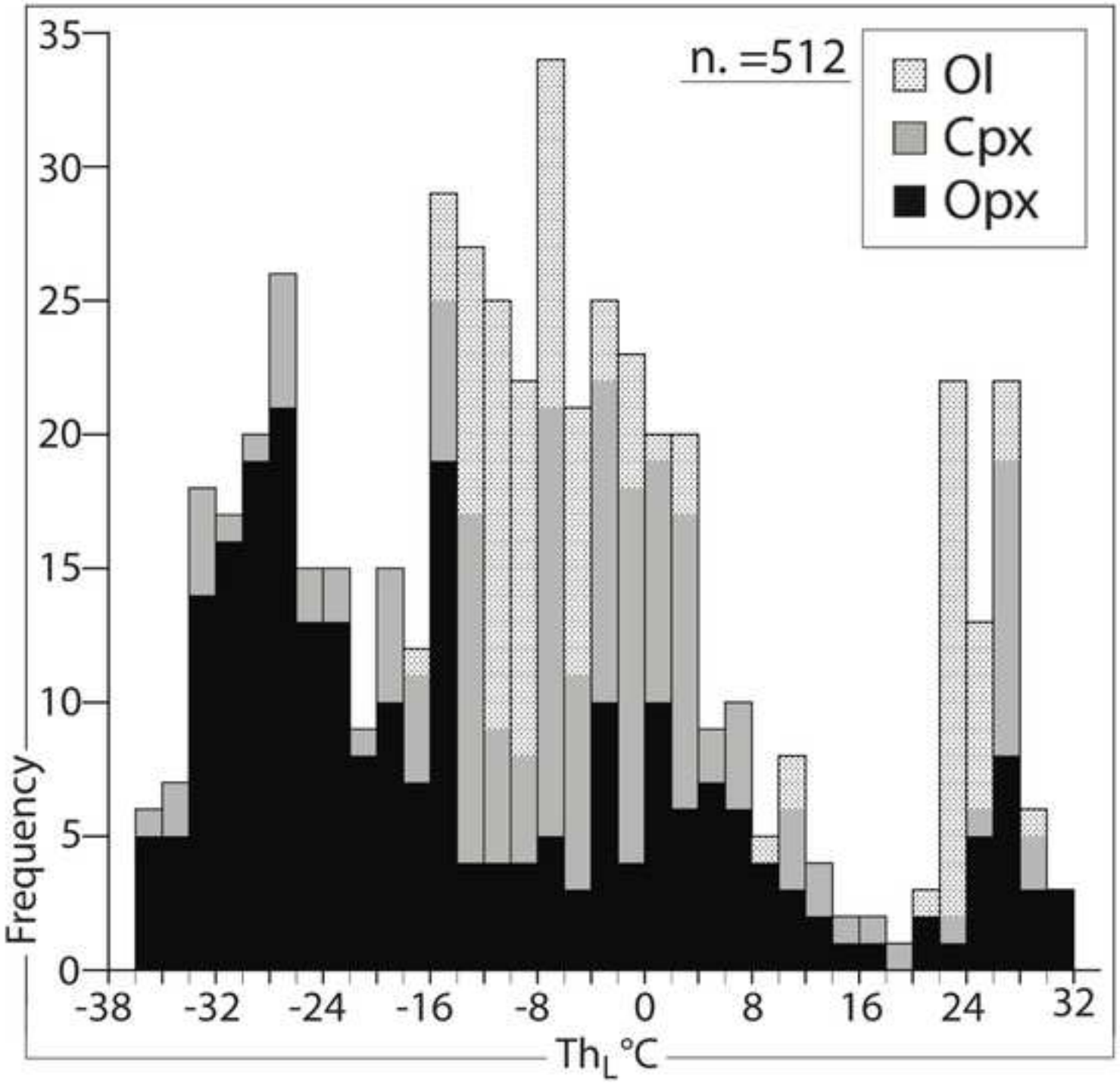

Fig.10.JPEG

Click here to download Figure Fig.10.jpg

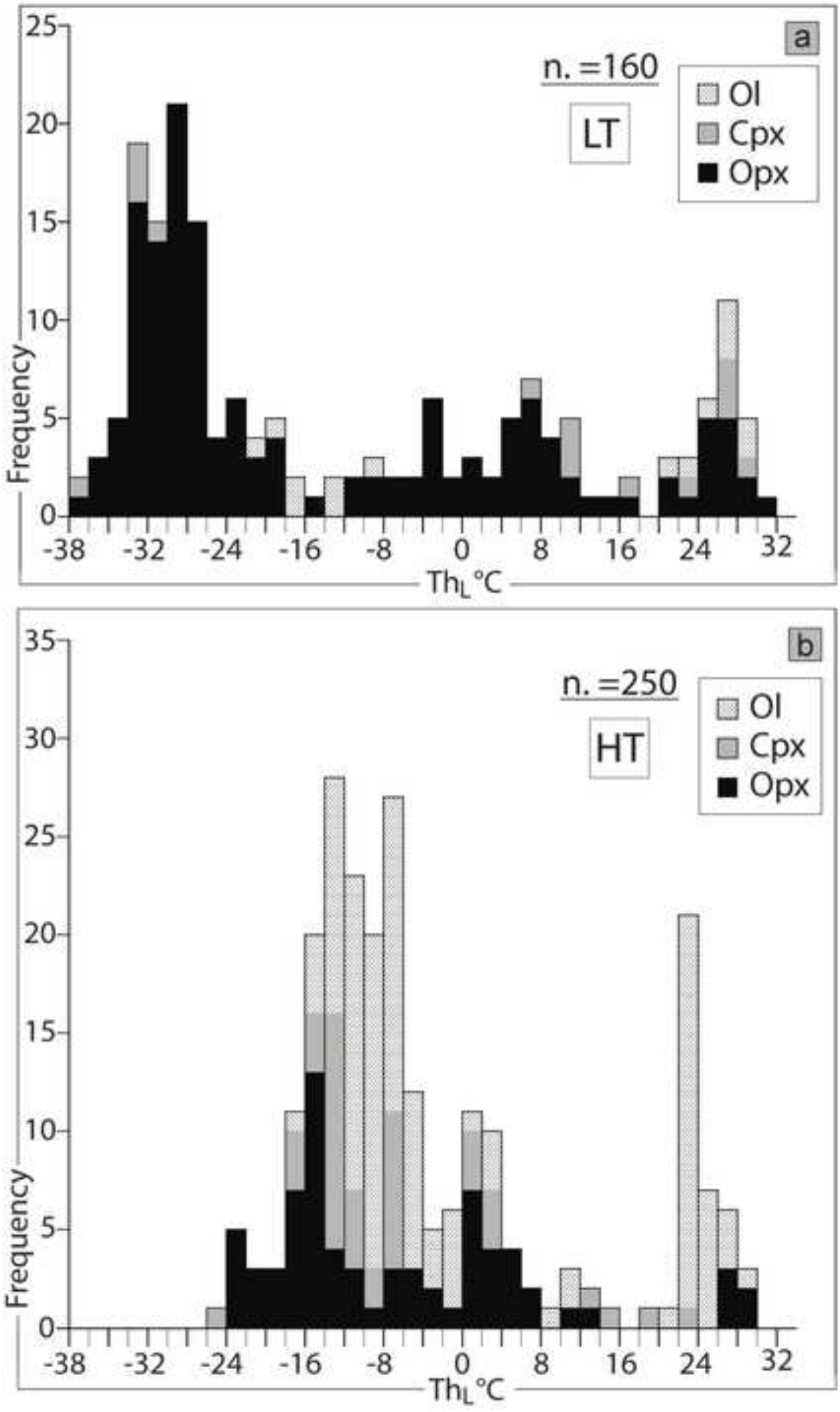

Fig.11.JPEG

Click here to download Figure Fig.11.jpg

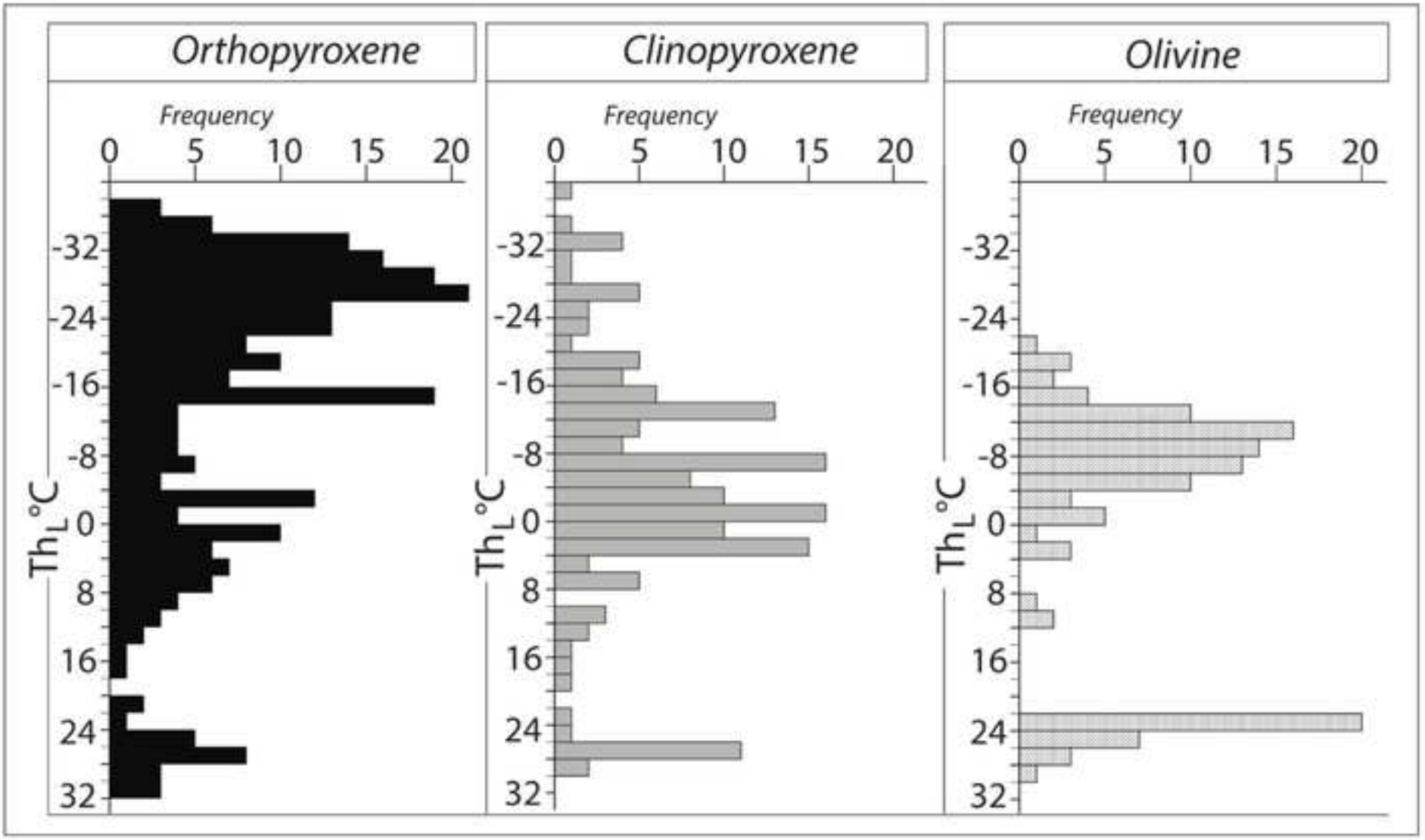

Fig.12.JPEG

Click here to download Figure Fig.12.jpg

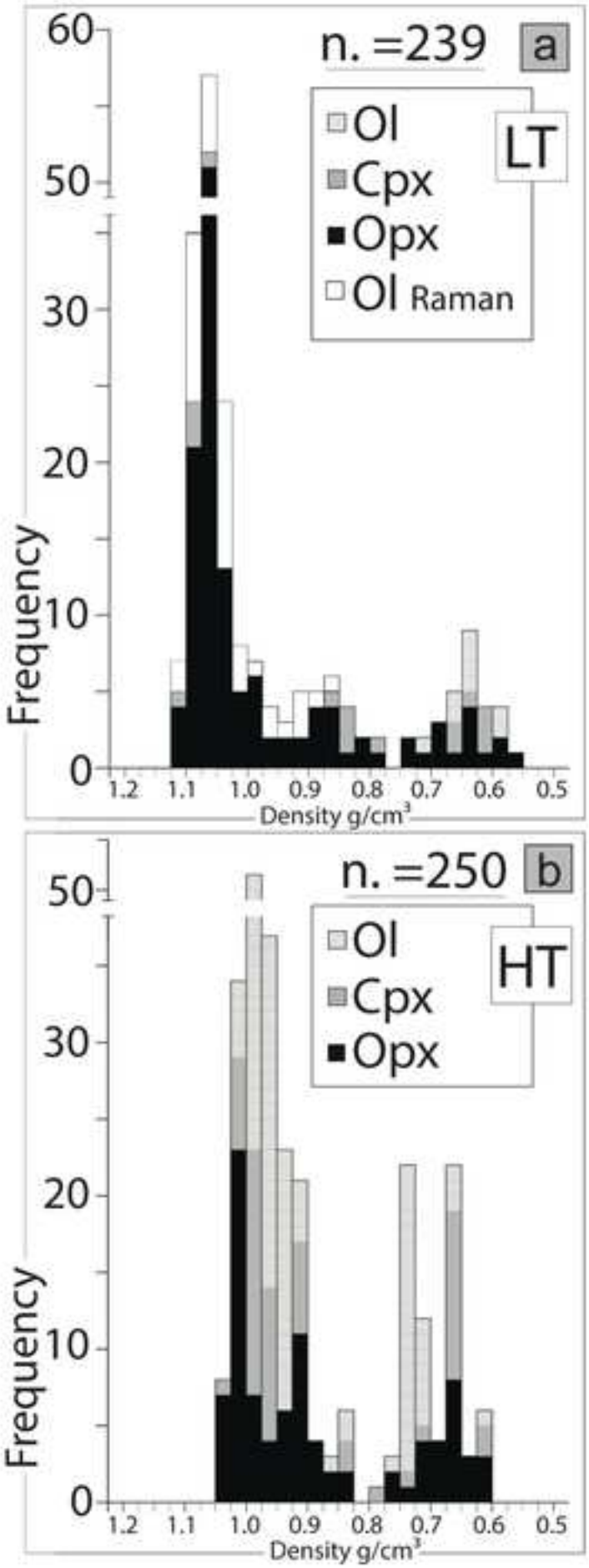

Fig.13.JPEG

Click here to download Figure Fig.13.jpg

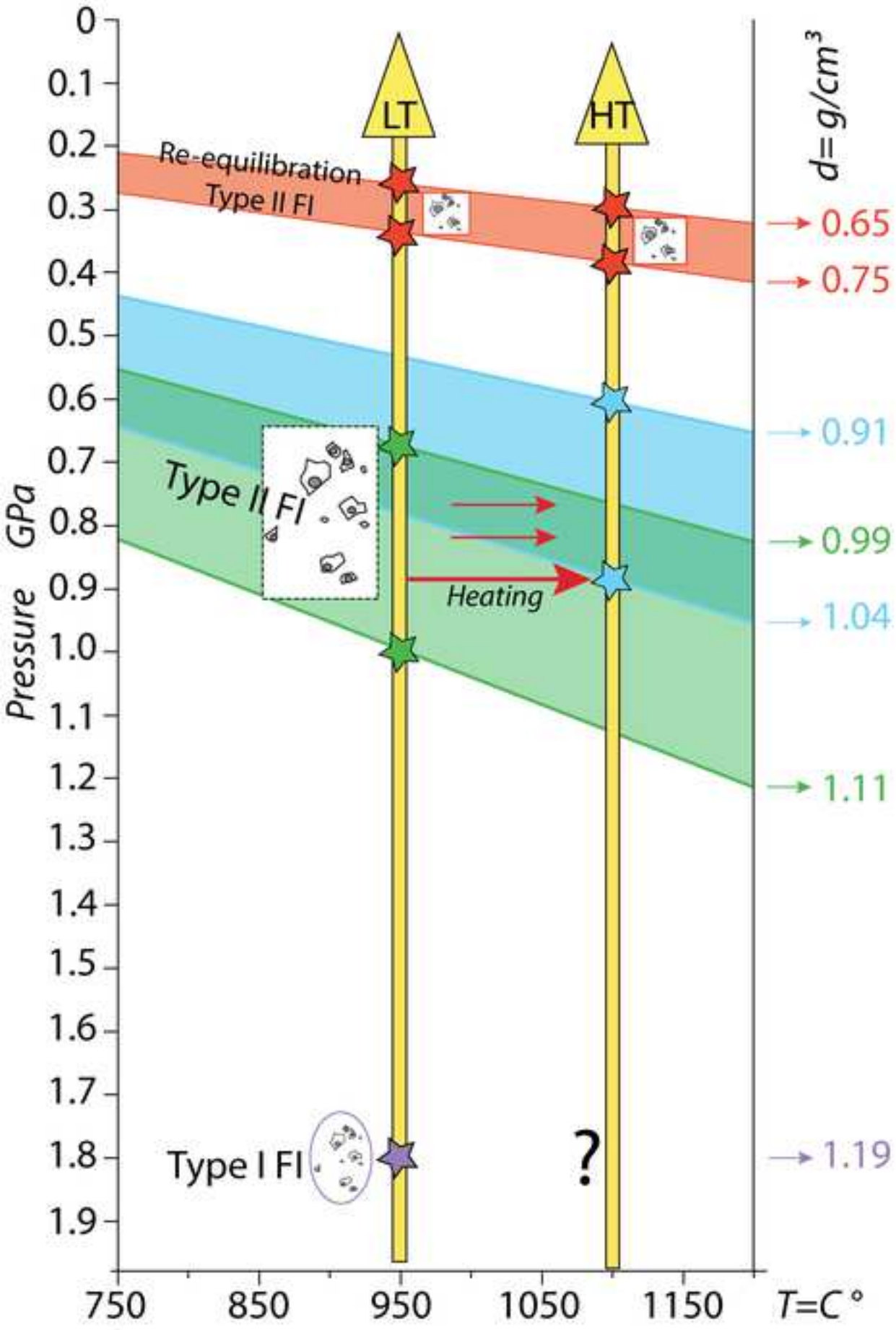

Fig.14.JPEG

Click here to download Figure Fig.14.jpg